Electric Field Poled Organic Electro-optic Materials: State of the Art and Future Prospects

Larry R. Dalton,* Philip A. Sullivan, and Denise H. Bale

Department of Chemistry, University of Washington, Seattle, Washington 98195

Received February 2, 2009

Contents

Larry R. Dalton received the B.S. and M.S. degrees in chemistry from the Honors College of Michigan State University with highest honors in 1965 and 1966. He received A.M. and Ph.D. degrees in chemistry from Harvard University in 1971. He is currently the George B. Kauffman University Professor of Chemistry and Electrical Engineering and the B. Seymour Rabinovitch Chair Professor of Chemistry at the University of Washington where he also directs the National Science Foundation Science and Technology Center on Materials and Devices for Information Technology Research. He is a senior member of IEEE and is also a Fellow of ACS, AAAS, SPIE-International Society of Optics and Photonics, and the Optical Society of America. Recent awards include a SPIE Lifetime Achievement Award, the IEEE/LEOS William Streifer Award, the American Chemical Society Award in the Chemistry of Materials, the American Chemical Society Southern California Section Richard C. Tolman Medal, and a Michigan State University Distinguished Alumni Award. He was honored in 2008 by the Dalton Festschrift Issue of the *Journal of Physical Chemistry*. Recent Federal Advisory Service includes the Defense Science Board Advisory Group on Electron Devices, the NSF Mathematical and Physical Sciences Directorate Advisory Committee, the Nanotechnology Technical Advisory Group of the President's Council of Advisors on Science and Technology, the Advisory Group for the Government Performance Act (NSF), and the Committees of Visitors of the Divisions of Materials Research and Chemistry of the National Science Foundation. He is the author or coauthor of over 600 scientific publications and patents.

1. Introduction

1.1. A Historical Perspective

Information is created, processed, transported, and detected using electrons, photons, phonons, or plasmons. Of these basic components of information technology, utilization of electrons and photons forms the practical basis of modern information technology. Electro-optics lies at the interface of these two important technologies (electronics and photonics) providing the means of converting information from the electronic domain to the photonic domain and vice versa. An example of such signal transduction is the encoding of digital (electronic) computer data onto the (optical or photonic) Internet. Initially, this was accomplished for telecommunication applications by use of modulated lasers, but as the need for higher bandwidth became evident in the late 1980s, focus turned to other faster response electro-optic (EO) technologies including inorganic crystalline electro-optic materials (such as lithium niobate), semiconductor electro-absorptive materials, and organic electro-optic materials. Of these various material technologies, organic electro-optic materials with extended π-electron conjugation afford the potential for the greatest bandwidth. The fundamental

* Fax: +1-206-616-8602. E-mail: dalton@chem.washington.edu.

10.1021/cr9000429
Published on Web 10/22/2009

Philip A. Sullivan received his B.S. (Honors) in Chemistry from Montana State University, Bozeman, in 2001 where he pursued undergraduate research in organic chemistry under the instruction of Cynthia K. McClure. He received his Ph.D. in Chemistry and Nanotechnology in 2006 from the University of Washington, while working with Larry R. Dalton. His dissertation was focused on the molecular engineering of organic materials for second-order nonlinear optical applications. He is currently a Research Assistant Professor of Chemistry at the University of Washington. Dr. Sullivan is the author or coauthor of more than 30 scientific publications and patents.

Denise H. Bale (Mushatt) received a B.S. degree in chemistry with Honors from Western Washington University, Bellingham, WA, in 2002. Her undergraduate honors work was conducted under Mark E. Bussell. She joined the research groups of Larry R. Dalton and Philip J. Reid at the University of Washington, Seattle, WA, where she completed her M.S. (2004) and Ph.D. (2008) degrees. She currently is carrying out research on the development and characterization of organic nonlinear optical materials under the guidance of Larry R. Dalton at the University of Washington.

response time of such materials (responding to a time-varying electric field) is the phase-relaxation time of the π-electron system (tens of femtoseconds, which can translate to potential bandwidths of tens of terahertz). In the late 1980s, the perceived need for faster time-division multiplexing (electrical-to-optical signal transduction and optical switching) led to a substantial industrial (IBM, DuPont, 3M, Hoechst-Celanese, Boeing, Lockheed Martin, etc.), Federal (DARPA, SDI/BMDO/MDA, etc.), and academic research effort. However, the advent of wavelength division multiplexing (WDM) dramatically reduced demands for high bandwidth time-division multiplexing. Telecommunication bandwidth requirements were also further impacted by the introduction of other multiplexing schemes including code division multiplexing. The late 1980s to early 1990s research efforts were also impacted by failure to achieve dramatic improvements in the properties of organic electro-optic materials. Electro-optic activity remained below the 30 pm/V value of lithium niobate (a material that secured its place as the dominant electro-optic material with refinements in crystal growth and device fabrication). Also, optical loss, thermal stability, and photochemical stability remained problematic and unanswered issues throughout the 1990s. By the late 1990s, most industrial research efforts had been abandoned with research at Lockheed Martin being one of the few exceptions. Federal funding focused explicitly on organic electro-optics also largely disappeared.

A 1994 thematic issue of Chemical Reviews[1] provides an excellent introduction to the research in electro-optics during the late 1980s and early 1990s. Indeed, a number of excellent reviews of research extending to 2000 have been published.[2−14] While many outstanding research groups contributed to the foundations of electro-optics, treatment of this early work would make this review overly long. Moreover, the research since 2000 deviates substantially in terms of material and device focus from the earlier work. In like manner, no attempt will be made to review the liquid crystal electro-optic literature; while liquid crystalline materials represent a critical display technology, the response times of such materials inhibit their use in telecommunications and high-speed information processing applications of primary interest here.

A few academic research programs focused on organic electro-optics did survive and were able to identify in the late 1990s and early 2000s structure−function relationships that led to dramatically improved electro-optic materials (improved molecular first hyperpolarizability, improved acentric order leading to improved macroscopic EO coefficients, and improved auxiliary properties such as optical loss and thermal and photochemical stability). The temporal evolution of device-relevant molecular first hyperpolarizability and macroscopic electro-optic activity for electrically poled organic materials is shown in Figure 1.[15] With respect to the improvement of molecular and macroscopic optical nonlinearity, the research efforts of the Dalton, Jen, and Robinson groups at the University of Washington and the Marks group at Northwestern University are particularly noteworthy. However, the recent resurgence of interest in organic electro-optic materials has also been motivated by a number of additional factors. Among these is a growing interest in photonic and electronic integration including chipscale integration, specific material requirements of emerging applications, and the demonstration of new device concepts and unique processing advantages of organic materials.

Electronic integration following Moore's Law and exploiting silicon complementary metal oxide semiconductor (CMOS) materials technology has afforded dramatic improvement in size, weight, and power (SWAP) requirements as well as cost, reliability, and performance of modern electronics. Realization of comparable advantages for photonic (and photonic/electronic) integration remains a grand challenge but one that could have a comparable transformative technological impact if successful. SWAP requirements are obviously of critical importance for airborne and space applications relevant to defense, sensing, and telecommunication, and dramatic improvements could be realized if chipscale integration could be achieved. The advent of silicon photonics has given new impetus to photonic integration because the high index of refraction of silicon permits reduction in the dimensions of photonic circuitry to scales

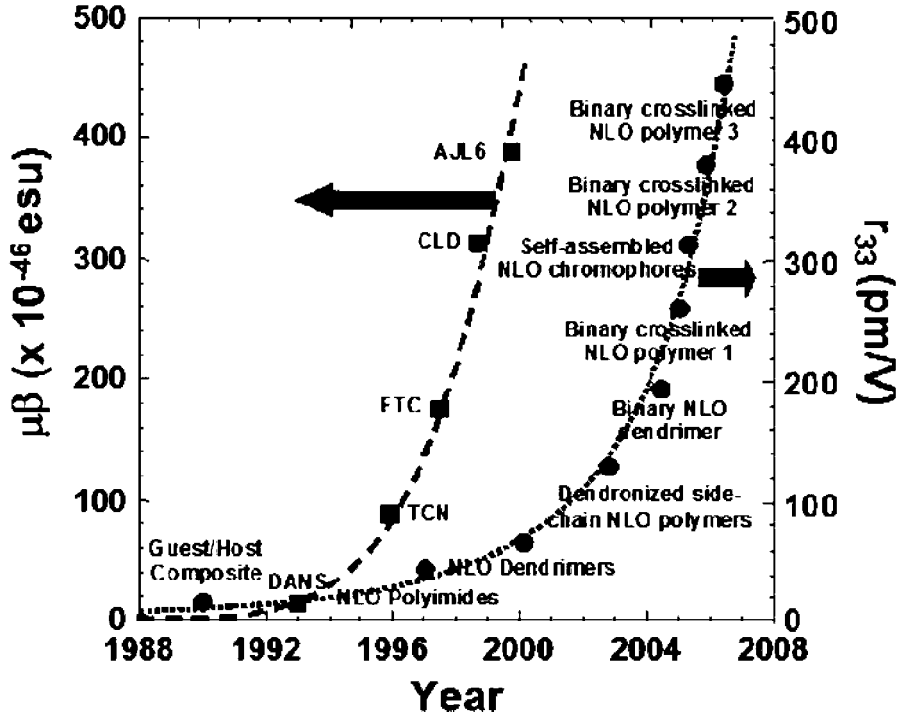

Figure 1. Temporal evolution of microscopic and macroscopic second-order nonlinear optical activity in poled organic materials. Reprinted with permission from ref 15. Copyright 2008 American Chemical Society.

more compatible with the dimensions of silicon CMOS electronic circuitry and permits greater flexibility in the design of photonic circuits.[16] The relatively high transparency of silicon at telecommunication wavelengths (e.g., centered around 1.3 and 1.55 μm wavelength) is another motivating factor in the rapidly growing interest in silicon as a photonic material. Initial problems with high optical (scattering) loss and the difficulty of realizing active control of light with silicon inhibited practical consideration of silicon in the late 1980s and early 1990s. However, since 2000, dramatic progress has been made addressing these issues and indeed even electro-optic modulation has been achieved with all-silicon devices.[17−20] Moreover, an advantage of organic electro-optic materials (namely, the ability to be integrated straightforwardly with disparate materials) has been demonstrated by the integration with silicon photonic waveguides including into nanoslots carved in such waveguides.[21,22] These recent advances have provided significant impetus to chipscale photonic integration, which could have dramatic impact on computing, telecommunications, transportation, medicine, sensing technologies (including infrastructure and environmental monitoring), and entertainment. Indeed, multifunctional devices such as the iPhone certainly reflect consumer interest in hand-held devices with multifunctional capability. Another motivator for chipscale integration is the realization of increasing advantages that can be achieved with respect to power requirements, cable density, areal density, edge density, and cost by using photonics rather than electronics for moving information various distances. The decision chart for choosing to use photonics rather than electronics (metal wire) to transport data is moving to ever shorter distances with time, reflecting the advantages that can be realized for these parameters by using photonics. Module-to-module integration using photonics is already common, and chipscale integration is an obvious next step, which is also being motivated by three-dimensional (chip stacking) integration.

Another essentially unique advantage of organic electro-optic materials is the ease of fabricating conformal and flexible devices[23] using these materials and in fabricating devices by a variety of processing options (solution, vapor phase) including soft and nanoimprint lithography[24] and various printing techniques (which are also recognized advantages of organic light-emitting device and electronic materials). A number of applications (e.g., phased-array antennae, optical gyroscopes, etc.) are greatly facilitated by the special properties of organic EO materials.

A final driver of the resurgence of interest in new electro-optic materials is application requirements that cannot be met with conventional electro-optic materials. For example, realization of gain in the electrical-to-optical-to-electrical conversion process of radio frequency (RF) photonics (distributing RF signals optically) is very critical to the field. Realization of gain requires an electro-optic V_π (voltage required to produce a π-phase shift of light) of about 0.1−0.2 V, which in turn, for reasonable device lengths and operational bandwidths, requires an electro-optic activity greater than 300 pm/V.[25] Energy consumption can also be a critical requirement, and organic electro-optic materials may permit dramatically reduced energy budgets in critical applications dependent on limited energy availability or suffering from thermal management problems. Finally, it can be noted that with video-on-demand, etc., bandwidth is yet again becoming an issue in telecommunications inspiring a revisiting of the use of organic materials. Indeed, the disparate SWAP, performance, cost, and reliability requirements of different applications are inspiring a broader search for new electro-optic materials to fulfill unsatisfied requirements.

While a number of remarks made in this review are applicable to crystalline organic electro-optic materials and to materials prepared by sequential synthesis/self-assembly, the focus of this review will be upon materials prepared by electric field poling.

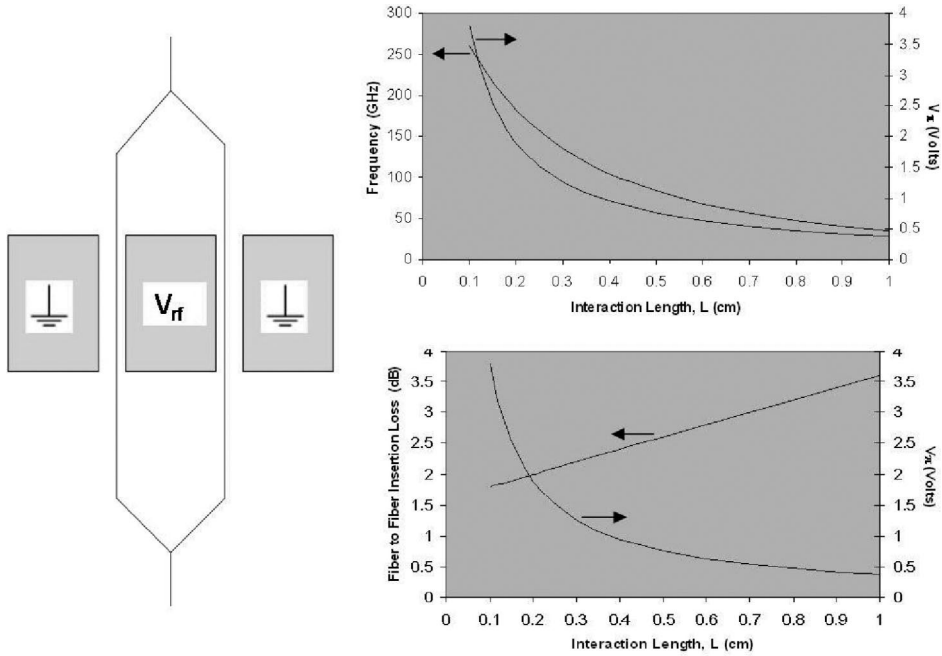

Figure 2. Schematic illustration (left) of a Mach−Zehnder interferometer. The relationship of switching speed, V_π, and optical interaction length (upper right); insertion loss, V_π, and interaction length (lower right), assuming $r_{33} = 300$ pm/V and propagation loss = 2 dB/cm.

1.2. Types of Materials and Device Requirements

Index of refraction of a material can be changed by heating the material (thermo-optic effect). This process is relatively slow and will not be discussed here. An electric field can also be used to change the collective orientation of liquid crystalline (LC) materials, but again this process is relatively slow because of the collective molecular mass that must be moved. The magnitude of index change that can be achieved with a given voltage is very large (corresponding to thousands of picometers per volt), but because of the slow speed, LC materials are not competitive for high-speed applications and will not be discussed further here. Semiconductor electro-absorptive materials (e.g., GaAs, InP) modulate light via an applied voltage that causes the wavelength of an optical resonance to change. The voltage required for modulation depends on the width of the resonance and can thus depend on the details of fabrication of material structures such as quantum dots. Both index of refraction (real part of the optical susceptibility) and absorbance (imaginary component of the optical susceptibility) change during electro-absorption modulation. This leads to the unwanted phenomenon of "chirp", which alters the signal (information) waveform. Optical loss is high for such materials because operation occurs near the half-maximum of absorption. Another mechanism of "electro-optic" modulation involving silicon derives from generation of a electron plasma by application of a voltage. This plasma perturbs the transmission of light and thus effects modulation. The major limitations of this method relate to bandwidth and thermal management because such devices run hot. Crystalline inorganic materials produce electro-optic modulation via ion displacement under the action of an electric field. Ion mass is intermediate between LC effective molecular mass and electronic mass of organic π-electron materials, so response time is intermediate. For inorganic materials, drive voltage and bandwidth are also limited by the velocity mismatch of propagating electrical and optical fields. This mismatch relates to the quantity $\varepsilon - \eta^2$ where ε is the dielectric permittivity and η is the index of refraction of a material. Velocity mismatch is not an issue for organic EO materials since $\varepsilon \approx \eta^2$. Let us now turn our attention to material requirements. For this discussion, we need to introduce at least basic categories of electro-optic devices.

Electro-optic devices can be divided into three general categories: (1) stripline (single-pass) devices such as Mach−Zehnder interferometers, directional couplers, and phase modulators;[24,26] (2) resonant (multipass) devices such as ring microresonators and etalons;[24,27] and (3) prism, cascaded prism, and superprism devices for applications such as beam steering and spatial light modulation.[28] The Mach−Zehnder interferometer (see Figure 2) is the prototype stripline device and is most commonly used to transduce an electrical signal onto an optical transmission as an amplitude modulation of the optical carrier. The voltage required to achieve full wave modulation is given by

$$V_\pi = \lambda d/(2\eta^3 r_{33} L\Gamma) \quad (1)$$

where r_{33} is the principle element of the electro-optic tensor, λ is the optical wavelength, η is the index of refraction, d is the electrode gap, L is the electrode length (interaction length of the electrical and optical fields), and Γ is the electrical/optical overlap integral. Bandwidth, drive voltage, and device insertion loss are all related through the length of device as is illustrated in Figure 2. For typical material parameters (resistivity of the gold electrodes (0.75 dB(GHz)$^{1/2}$ per cm), activity of the EO material (300 pm/V), and optical loss of the EO material (2 dB/cm)), a 0.5 cm long device exhibits a V_π of 0.75 V, a bandwidth of 90 GHz, and an insertion loss of 2.6 dB. Unless the EO activity is increased from 300 pm/V (of this example), realization of a drive voltage of 0.2 V would require a device length of 1.9 cm, which would increase the insertion loss to 5.4 dB. From this simple example, it is clear that different bandwidth, drive voltage, and insertion loss requirements will mandate different material requirements.

The ring microresonator can be considered to be a prototype structure for resonant devices. Only certain wave-

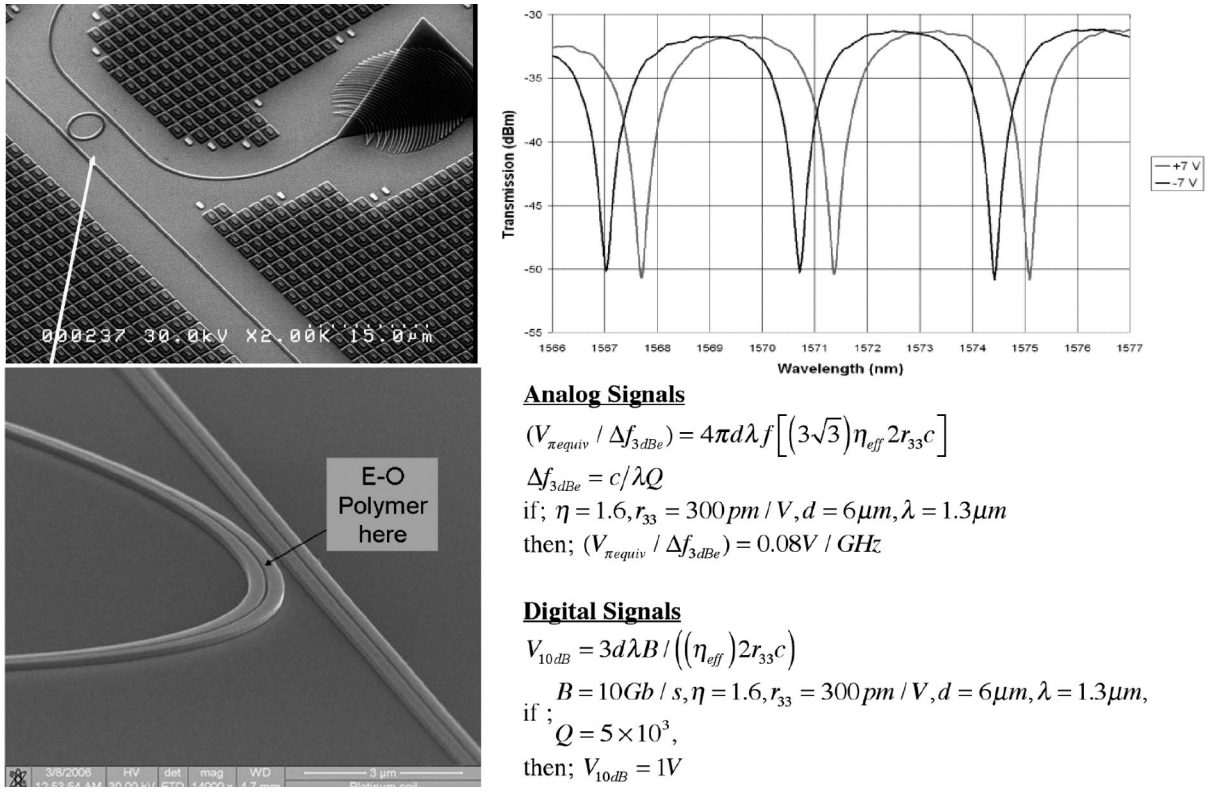

Figure 3. Micrograph images of microring-resonator devices fabricated in silicon (left) and ring-resonator operational parameters (right).[21,22,219]

lengths of light are coupled into the ring to form standing waves in a ring microresonator with the selection criteria defined by the effective ring circumference ($\eta_{\text{eff}}L$) and the index of refraction difference between the input and ring waveguides (the optical impedance matching condition) as governed by

$$\lambda = \eta_{\text{eff}}L/m \tag{2}$$

where η_{eff} is the effective index of refraction, L is the path length around the ring, and m is an integer. The number of times that light transits the ring before being lost is defined by optical loss mechanisms, that is, by the quality (Q) factor [Unloaded $Q = 2.73 \times 10^5\eta_{\text{eff}}/(\alpha\lambda)$ where α is the sum of all loss mechanisms (material, bending, and scattering due to wall roughness of the ring)]. The Q factor defines the effective path length over which the optical and electrical signals interact (i.e., the number of times that a photon circumnavigates the ring). Q is also given by $\omega/\Delta\omega$, where ω is the optical frequency and $\Delta\omega$ is the width of the pass band. The higher the Q, the lower V_π is required for modulation and switching, but Q also defines bandwidth by fixing the photon lifetime in the ring. Bandwidth and voltage (sensitivity) are explicitly related by the bandwidth/voltage sensitivity factor (BW)

$$\text{BW} = (\Delta\nu_{\text{fwhm}})/V_{\text{fwhm}} = K\nu\eta^3 r_{33}/(2\eta_{\text{eff}}d) \tag{3}$$

where V_{fwhm} is the voltage required to shift the resonance an amount equal to the resonance width at half-maximum, K is the confinement factor, η is the refractive index of the EO material, η_{eff} is the effective refractive index of the ring, and d is the electrode spacing. Since a microring resonator selects certain wavelengths for transmission, it can be considered a voltage-controlled filter or a device for active wavelength division multiplexing (color-coding of information). Obviously, from a consideration of Figure 2, it is easily realized that microrings can be used as voltage-controlled optical routing switches (reconfigurable add/drop optical multiplexer, ROADM). Finally, electrical information can be encoded on the optical beam in the ring indicating the third common use of microring resonators.

The analysis of ring microresonator performance differs somewhat for digital and analog data as is shown in Figure 3. From consideration of this figure, it is clear that electro-optic activity greater than 300 pm/V is critical for many applications.

The discussion of superprism (and photonic bandgap or crystal) devices is beyond the scope of this review, but the relationship between drive voltage and material parameters for prism and cascaded prism devices (spatial light modulators) is given by

$$\theta = (\eta)^3 r_{33}(VL/(dh)) \tag{4}$$

where L and h are the length and width of the prism or the array of prisms, V is the voltage applied across an overall thickness d (or the electrode spacing), and θ is the deflection or beam steering angle (see Figure 4).[28] The effective interaction length between electrical and optical fields can be increased using a cascaded prism device (rather than a simple single prism) structure where the effective length L is given by the length of the base of the prism cascade.[28] However, even for cascaded prism devices, it is very important to have a large electro-optic coefficient to achieve large-angle spatial light modulation with acceptable drive voltages.

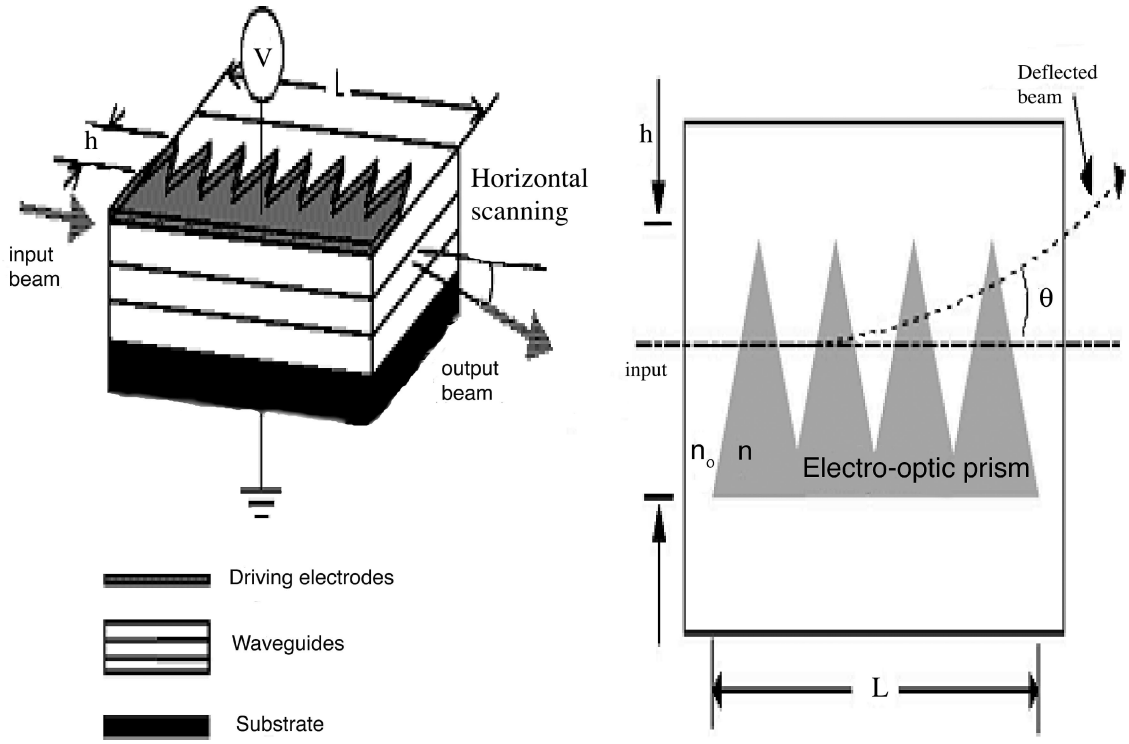

Figure 4. Diagram of a superprism (spatial light modulator). Reprinted with permission from ref 28. Copyright 2001 SPIE.

2. The Electro-optic Effect and Organic EO Materials

2.1. The Electro-optic Effect

Organic EO materials consist of many nonlinear optically active molecular units (chromophores) combined to create a bulk material. Chromophores are materials with extended π-electron conjugation in which the delocalized electron density may be polarized easily in response to an applied electric field. These chromophores may be combined in pure form or dispersed throughout an optically inactive (transparent) matrix such as a polymer or dendrimer. In the case of an isolated chromophore, the polarization, p, of electron density that occurs in response to a relatively weak electromagnetic field may be described by the relation

$$p = p_0 + \alpha_{ij}E_j \tag{5}$$

where p_0 represents the equilibrium polarization, α_{ij} denotes a particular tensor element of the linear polarizability, and E_j is a vector component of the applied electric field. In bulk media, the analogous description becomes

$$P = P_0 + \chi_{ij}^{(1)}E_j \tag{6}$$

where $\chi_{ij}^{(1)}$ represents linear susceptibility. When an optical field of a particular frequency interacts linearly with a material, the material exhibits a time varying polarization response proportional to the intensity. This response serves to alter the incident field in such a way as to create a new field that is of the same frequency, but the propagating wave is phase-shifted in time with respect to the incident field. The magnitude of this phase shift is proportional to the index of refraction, η, of the material.

When an adequately intense optical field, such as laser radiation, interacts with the material, eq 6 is no longer sufficient to describe the response. The description must now be expanded to include nonlinear (higher order) polarization terms. On the single molecule level, the description now becomes

$$p = p_0 + \alpha_{ij}E_j + \beta_{ijk}E_jE_k + \gamma_{ijkl}E_jE_kE_l \tag{7}$$

where β_{ijk} and γ_{ijkl} denote the chromophore first and second hyperpolarizabilities, respectively. Again, a power series expansion analogous to the single molecule description can be applied to the bulk level:

$$P = P_0 + \chi_{ij}^{(1)}E_j + \chi_{ijk}^{(2)}E_jE_k + \chi_{ijkl}^{(3)}E_jE_kE_l \tag{8}$$

where $\chi_{ijk}^{(2)}$ and $\chi_{ijkl}^{(3)}$ denote the first and second nonlinear susceptibilities. Unlike the linear case, time-varying nonlinear polarization effects give rise to new fields of altered frequency with respect to the incident radiation. This phenomenon results in second harmonic generation (SHG) in the case of $\chi_{ijk}^{(2)}$ and third harmonic generation (THG) in the case of $\chi_{ijkl}^{(3)}$. In addition to frequency alteration in the form of SHG, first nonlinear susceptibility, $\chi_{ijk}^{(2)}$, gives rise to an electric field dependent effective (combined) susceptibility. This accounts for the Pockels (or linear electro-optic) effect in which control of electromagnetic susceptibility and refractive index is effected by application of a low-frequency (DC-10 THz) electric field (i.e., low-frequency with respect to the optical field; $\lambda = 1.55$ μm; $\omega = 1.9 \times 10^{14}$ Hz).

Unlike odd-order susceptibility terms, a nonzero $\chi_{ijk}^{(2)}$ requires net asymmetry. In a bulk material that is constructed from many molecularly asymmetric (dipolar) chromophores, this need for overall noncentrosymmetry imposes the additional requirement of molecular alignment in order to achieve a finite macroscopic second-order nonlinear optical activity. In a real material, in which the molecular constituents are imperfectly aligned, $\chi_{zzz}^{(2)}(\omega)$ (the principle element of the nonlinear susceptibility tensor at frequency ω) is related to the molecular parameters by

$$\chi^{(2)}_{zzz}(\omega) = N\beta_{zzz}(\omega,\varepsilon)\langle\cos^3\theta\rangle g(\omega) \quad (9)$$

where N (molecules/cm^3) denotes the number density of active molecules that interact with the incident optical field, β_{zzz} is the hyperpolarizability tensor element coincident with the molecular symmetry axis, which is dependent on the wavelength (frequency)[2,29] of the incident light field, ω, and the dielectric permittivity of the electro-optic material, ε.[30−32] The $\langle\cos^3\theta\rangle$ term is the average molecular acentric order parameter denoting the extent of chromophore alignment relative to the laboratory z axis. The z laboratory axis is parallel to the applied poling field (in electric field poled materials), as well as the field vectors of the optical and electrical operating fields in the case of an EO device. The quantity $g(\omega)$ is the Lorentz−Onsager local field factor.[8,29] The dominant element of the linear Pockels EO effect tensor, r_{33}, denotes the magnitude of phase (refractive index, $\Delta\eta$) shift obtained for an applied low-frequency electric field and is given in units of pm/V. This EO coefficient is related to $\chi^{(2)}_{zzz}(\omega)$ by

$$r_{33}(\omega) = \frac{-2\chi^{(2)}_{zzz}(\omega)}{\eta^4} \quad (10)$$

where η is the refractive index of the EO material.

Equation 9 demonstrates the three most important factors in the optimization of $\chi^{(2)}_{zzz}(\omega)$ and, in turn, $r_{33}(\omega)$: Chromophore number density, molecular first hyperpolarizability, and acentric order must be maximized simultaneously. In the case of π-conjugated dipolar molecules, $\beta_{zzz}(\omega,\varepsilon)$ is largely determined by molecular composition and can be tuned using synthetic chemistry guided by theoretical modeling. Unfortunately, due to strong interchromophore electrostatic interactions N and $\langle\cos^3\theta\rangle$ are not independent. As the density of the highly dipolar chromophores increases, the average distance between them decreases and strong dipole−dipole interactions begin to compete with ordering forces such as the poling field.[33−36] Therefore, the product, $N\langle\cos^3\theta\rangle$, termed the loading parameter, must be optimized using theory-guided molecular engineering approaches to control chromophore shape, lattice attachment geometry, solubility, etc. Recently, great progress has been made in enhancing r_{33} through the use of coupled quantum and statistical mechanical modeling to guide the improvement of both $\beta_{zzz}(\omega,\varepsilon)$ and $N\langle\cos^3\theta\rangle$.[36]

2.2. Optimization of Molecular Hyperpolarizability

Optimization of the molecular first hyperpolarizability, $\beta_{zzz}(\omega,\varepsilon)$, of dipolar EO chromophores relies on tuning of the electron density distribution through chemical modification of molecular constituents. Ground-state electron density asymmetry, necessary for $\beta_{zzz}(\omega,\varepsilon)$, is induced through the asymmetric substitution of a π-electron-conjugated bridge with the appropriate donor and acceptor moieties.

Figure 5 illustrates electron density asymmetry in a chromophore composed of a triaryl amine donor, thienyl vinylene bridge, and 2-(3-cyano-4,5-dimethyl-5-trifluoromethyl-5*H*-furan-2-ylidene)-malonitrile (CF_3-TCF) acceptor.[37] As a general rule, stronger electron density donors and acceptors and increased conjugated bridge length lead to larger $\beta_{zzz}(\omega,\varepsilon)$. This rule holds well for chromophores constructed using an aromatic bridge segment that somewhat energetically impedes polarization. However, in the case of highly polarizable polyene (energetically degenerate ground-state double bond configurations) bridge structures, an optimum donor/acceptor match exists. This phenomenon may be best understood by considering a two-state theoretical approximation for the dependence of the principal nonresonant hyperpolarizability tensor element (oriented along the dipolar axis) on the contributions from frontier orbitals. This approximation for β_{zzz} can be expressed as

$$\beta_{zzz} \propto \frac{\Delta\mu_{eg}(\mu_{ge})^2}{E_{ge}^{\ 2}} \quad (11)$$

where $\Delta\mu_{eg}$ represents the difference in dipole moment between the highest occupied (HOMO) and the lowest unoccupied (LUMO) molecular orbitals, μ_{ge} represents the transition dipole moment (oscillator strength) and E_{ge} represents the energy difference between ground (HOMO) and charge transfer excited states (LUMO).[38−40] As donor and acceptor strength initially increases, hyperpolarizability increases up to an optimum value. Past this optimum, the electron density begins to be symmetrically distributed along the molecular long axis until $\Delta\mu_{eg} \approx 0$ and thus β_{zzz} disappears and the dye assumes cyanine-like electron density distribution. If the donor/acceptor strength is increased further, this cyanine-like state again becomes asymmetrically polarized with the electron density now shifted to the acceptor, creating a charge-separated (zwitterionic) state. In this case, the HOMO and LUMO effectively switch orientation. In such a situation, $\Delta\mu_{eg}$ and β_{zzz} become negative. This behavior may also be understood in terms of bond length alternation (BLA).[41,42]

The simplistic two-state model can be a useful tool to guide the work of synthetic chemists. However, because of the complicated contributions to effective hyperpolarizability from chromophore constituent alteration and environmental effects, quantum mechanical computer modeling has been recognized as extremely valuable. Density functional theory (DFT) allows evaluation of the entire $\boldsymbol{\beta}$ tensor using the finite field method.[43−45] Additionally, sum-over-states methods have also been extensively employed for evaluation of molecular hyperpolarizability and dipole moment.[46−50] Several reports comparing molecular nonlinearity computations also exist.[51,52] DFT methods have proven accurate and can be readily extended to include frequency (operational wavelength) dispersion effects as well as environmental dielectric dependence.[53] In order to accurately predict the nonlinear behavior of a chromophore structure, consideration of environmental ε must also be included. Reaction field DFT studies (Dmol^3 PBE/DNP/COSMO) coupled with hyper-Rayleigh scattering (HRS) and electric field induced second harmonic generation (EFISH) measurements in different solvents have confirmed that $\beta_{zzz}(\omega,\varepsilon)$ can vary by as much as a factor of 4 between vacuum and high ε solvent environments. In addition to hyperpolarizabilty, properties such as refractive index, dielectric constant, and absorption spectra may be obtained as a function of frequency.

The dependence of hyperpolarizability on the proximity of the optical resonance frequency, ω_{ge} (λ_{max} for optical absorption and E_{ge} in eq 11), and the frequency (wavelength) of the incident optical field is discussed below. Figure 6a demonstrates the relationship between the real, η (refraction), and imaginary part, κ (absorption), of the complex refractive index where $\eta + i\kappa = \eta_c \propto \chi^{(1)}$ for a multichromophore dendrimer thin film.[54] Figure 6b illustrates the frequency

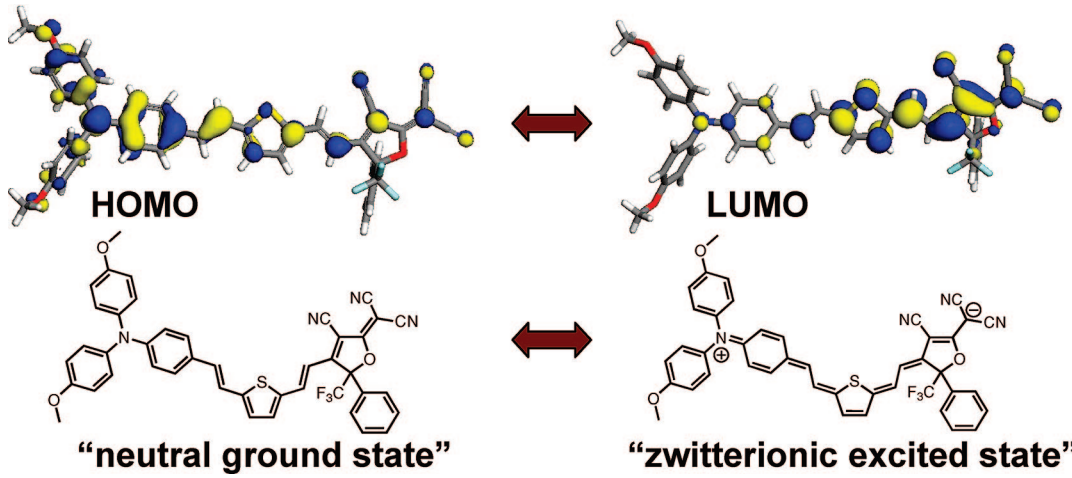

Figure 5. Density functional theory (DFT) computer modeling generated electron density surface depiction (top) of the highest occupied molecular orbital (HOMO) and lowest unoccupied molecular orbital (LUMO) of a triaryl amine donor/tricyanovinylfuran acceptor EO chromophore and corresponding chemical structure depiction (bottom) of neutral ground and zwitterionic Mulliken charge transfer states.

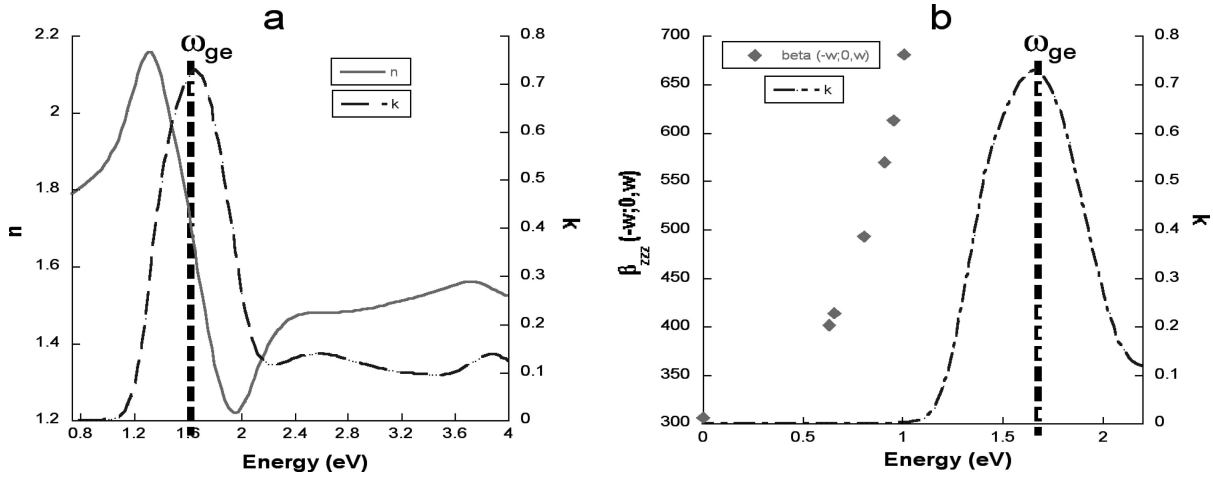

Figure 6. (a) The relationship between the real, η, and imaginary, κ, contributions to the complex refractive index of a three-arm dendronized chromophore film and (b) the predicted relationship between $\beta_{zzz}(\omega,\varepsilon)$ in a vacuum and the chromophore absorption (resonance) calculated using real-time time-dependent density functional theory (RT-TDDFT) methods.

dependence of $\beta_{zzz}(\omega,\varepsilon)$ and its relationship to optical absorption and ω_{ge}. Here, $\beta_{zzz}(\omega,\varepsilon)$ was calculated using real-time time-dependent density functional theory (RT-TDDFT) computational methods.[44] Both η and $\beta_{zzz}(\omega,\varepsilon)$ display a pronounced increase as ω_{ge} is approached from the low-energy side. As a result, when the HOMO to LUMO energy gap is shifted closer to the energy of the operational light field, polarizability and hyperpolarizability are enhanced. Stronger donors and acceptors, in combination with longer bridges, result in a reduced HOMO−LUMO energy gap and an optical absorption shifted toward longer wavelengths and lower frequencies. Because of the low propagation loss of near-infrared light in optical fibers and the availability of light sources, the most common wavelengths used by the telecommunications industry are $\lambda = 1.55\ \mu$m, $\omega = 1.9 \times 10^{14}$ Hz and $\lambda = 1.3\ \mu$m, $\omega = 2.3 \times 10^{14}$ Hz. Current state-of-the-art EO chromophores can have optical absorption maxima of $\lambda_{max} = 0.75-0.8\ \mu$m with absorption band edges extending almost to $\lambda = 1\ \mu$m. Due to the potentially reduced photochemical stability and high optical loss associated with increased optical absorption, simply driving the chromophore absorption maxima to lower energies is not a good strategy for enhancing r_{33}.

2.3. Optimization of Bulk Electro-optic Activity

In order to achieve a large r_{33} value, high microscopic nonlinearity must be accompanied by high acentric chromophore order. Methods for the induction of molecular order have included electric field poling, in which an initially isotropic material is ordered by application of a large DC electric field while the material is heated, and sequential synthesis, self-assembly methods in which molecular order is induced through layer-by-layer assembly exploiting either ionic (Langmuir−Blodgett) or covalent (Merrifield) spatially anisotropic interactions. Because of the requirement for molecular order on the micrometer scale (several thousand times the length of an individual molecular layer), self-assembly using sequential synthesis or other layer-by-layer deposition techniques has been largely seen as impractical. New developments, such as hybrid silicon nanophotonic/organic electro-optic devices[21,22] in which required dimensions are greatly reduced, may provide a good platform for the application of these techniques. For a detailed discussion of self-assembled EO materials, the reader is referred elsewhere.[55,56]

Electric field poling has remained by far the most widely studied technique for the induction of bulk chromophore

order. In the case of electric field poling of materials created by embedding of dipolar EO chromophores into host matrices, acentric molecular order is induced by heating the initially isotropic guest/host material to just below the glass transition temperature under the application of a large DC electric field. At this temperature, the chromophores possess enough thermal energy to be mobile within the material matrix and their permanent dipole moments respond to oppose the poling field resulting in unidirectional molecular order. In this case, simple inspection of eqs 9 and 10 suggests that $\chi^{(2)}_{zzz}(\omega)$ and r_{33} should increase linearly with N if all other parameters are held constant. Experimentally, as N increases, an optimum chromophore concentration becomes apparent, beyond which r_{33} begins to fall.[33,34] Because of this "roll-off" behavior, it is necessary to consider the $N\langle\cos^3\theta\rangle$ product in order to optimize r_{33}.

In order to understand this dependence of order on chromophore number density, we begin by examining the orientation (by the application of an electric field) of non-interacting dipolar molecules in the gas phase. This ordering behavior can be described by

$$\langle\cos^3\theta\rangle = L_3(f) \tag{12}$$

where L_n is the third-order Langevin function and $f = \mu F/(kT)$. Here, F is the poling field felt by the chromophore, μ is the permanent (ground-state) dipole moment, k is the Boltzmann constant, and T is the poling temperature (kelvin). At very low values of $f \ll 1$, the expression for field-induced order simply becomes

$$\langle\cos^3\theta\rangle = \mu F/5kT \tag{13}$$

Here, order is independent of N. However, when dipole−dipole intermolecular electrostatic interactions (in the point dipole approximation) are included, the reason for the roll-off behavior becomes apparent. Using the approach of Piekara,[57] the details of the vector quantities relating the orientation of all neighboring chromophore dipoles to the field felt by any single chromophore may be replaced by the mean field. This simplified approach results in the inclusion of an attenuation factor related to the ratio of the total electrostatic energy, W, and the thermal energy, kT. Equation 8 now becomes

$$\langle\cos^3\theta\rangle = L_3(f)\{1 - [L_1(W/(kT))]^2\} \tag{14}$$

where the attenuation factor $\{1 - [L_1(W/(kT))]^2\}$ serves to counteract the poling field. As μ or N increases, W becomes larger and the attenuation factor eventually begins to override the poling field.

The discussion thus far has treated chromophores only as point dipoles without shape or size. In this case, $N\langle\cos^3\theta\rangle$ only depends on the value of μ and the average distance between dipoles. However, because the dipole moment is a vector quantity and W is inversely proportional to the distance between dipolar units, molecular size and shape certainly have an impact. In order to better understand the material design factors, such as molecular shape, that impact the extent of dipolar order obtained through the application of a given poling field, E_p (V/μm), atomistic computer simulations have been developed.[58−62] In order to reduce the computational expense of fully atomistic simulations "pseudo-atomistic" Monte Carlo methods (PAMC) have been adopted.[34,36,63] In this approach, π-conjugated molecular segments (such as the chromophore backbone) are treated as rigid ellipsoid shapes. DFT methods are then used to define the dipole moment. All σ-bond segments are treated fully atomistically.

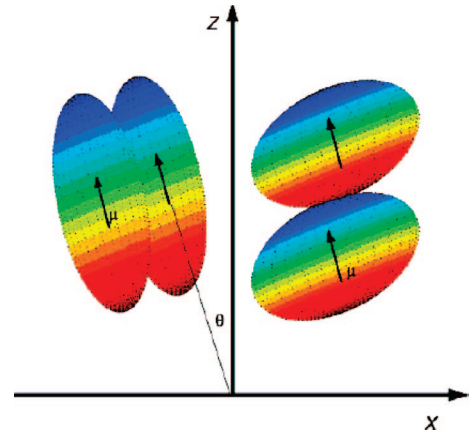

Figure 7. Illustration of the side−side packing behavior of 1:2 aspect ratio prolate ellipsoids (left) and the head−tail packing behavior of 2:1 aspect ratio oblate ellipsoids (right). Reprinted with permission from ref 63. Copyright 2007 American Chemical Society.

Figure 7 illustrates how chromophore shape influences electrostatic interactions and $N\langle\cos^3\theta\rangle$. Prolate ellipsoids with a 1:2 (width/length) aspect ratio are shown on the left. The long and thin shape of these molecules favors side-to-side interaction in which electrostatics will energetically disfavor acentric (poling-induced) order. In contrast, oblate (disk-like) spheroids with a 2:1 aspect ratio will disfavor side-to-side intermolecular interactions and favor head-to-tail interactions. If the electric field ordering of oblate spheroids is simulated only allowing the molecules to rotate and not spatially translate, the favored head-to-tail dipolar forces are predicted to drive acentric order. This model is termed "on-lattice".[63] However, as Figure 8 illustrates, when the dipolar oblate spheroids are allowed to translate (a more realistic "off-lattice" model) as well as rotate in order to minimize the energy of the system, $N\langle\cos^3\theta\rangle$ vs N is predicted to be poorer than that of prolate ellipsoids and spheres (Figure 8, right). The cause of this seeming discrepancy lies in the fact that the condensed phase is initially created in the absence of a poling field. The molecules making up this solid material are thus able to rotate, translate, and aggregate, into isotropically organized noncentrosymmetric molecular domains (Figure 8, left). Even though these domains possess order on the scale of several molecules, no net order exists in the bulk. When a poling field is applied, very little response ensues due to the higher energy required to break and reorder these aggregates. From this type of modeling, it is predicted that at high molecular density, a chromophore that is spherical in shape allows the highest $N\langle\cos^3\theta\rangle$ for a given poling field strength. The oblate shape presents possibilities for short-range self-assembly that may be templated by a dipolar surface layer and grown sequentially. Such materials might find application in new device architectures, such as hybrid silicon photonic/organic EO nanoscale photonic devices, that do not require micrometer-thick ordered films.

For reference, for a highly dipolar prolate EO chromophore (typical of the unmodified chromophores discussed herein), PAMC modeling predicts that a molecular ensemble, having a number density in the range of $N \approx (0.5-7.0) \times 10^{20}$ molecules/cm^3, under an applied poling field of $E_{pol} = 150$

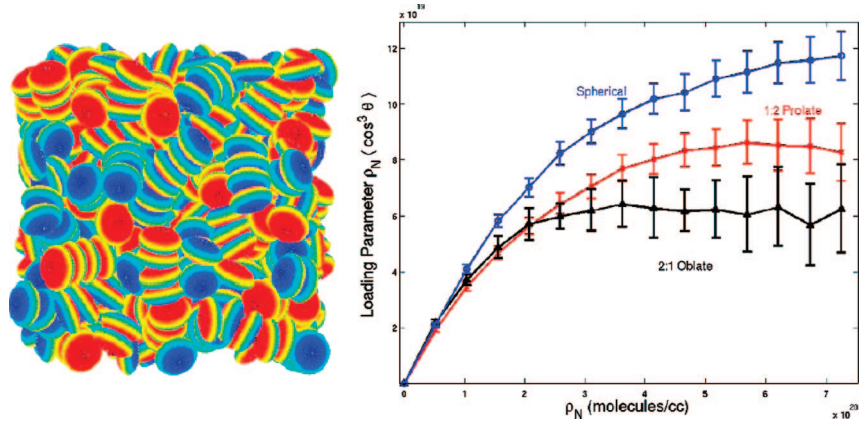

Figure 8. "Off-lattice" simulation (right) for $N\langle\cos^3\theta\rangle$ for spherical (1:1), prolate (1:2), and oblate (1:3) aspect ratio dipolar shapes as a function of number density and "snapshot" of electric field induced ordering (left) of oblate spheroids at high density. Reprinted with permission from ref 63. Copyright 2007 American Chemical Society.

V/μm, will yield the commensurate range of order parameters; $\langle\cos^3\theta\rangle \approx 0.4-0.2$ (decreasing with increasing N).[63]

2.4. Optimization of Auxiliary Properties

In order for organic EO materials to realize widespread commercial application, several practical requirements must be satisfied in addition to high r_{33}. In particular, the nonlinear properties of the material must be stable under operating conditions that include high optical intensity, elevated temperatures, and potentially high-energy radiation (γ rays and energetic protons in the case of space-based applications). These requirements emphasize the need for a material to display thermal, mechanical, and photochemical stability and low optical loss, in addition to large optical nonlinearity.

In order for r_{33} to exhibit high temporal stability at elevated operating temperatures, chromophore alignment induced during the poling process must be stable. Because the poling process relies on the application of electromotive force to induce order in an initially randomly ordered material, the resulting order is energetically disfavored. Therefore, in the absence of the poling field, poled order relaxes back to the isotropic state as a function of time and temperature. Like poling, the specifics of relaxation (rate) are closely related to T_g.[64] Increased molecular reorientation rates at elevated temperatures allow poling to take place, but if no mechanism is present to slow reorientation after poling, elevated temperature serves to accelerate relaxation and r_{33} decay. Many successful cross-linking (lattice hardening) methodologies have been demonstrated that dramatically improve temporal stability at elevated operating temperatures by increasing the activation energy required for molecular motion. Cross-linking is discussed in more detail in section 4.2.

Photostability at operating (telecommunications) wavelengths, $r_{33}(\omega)$, and optical loss[65] are interrelated by the proximity of λ_{max} (and the low-energy side (red-edge) of absorption band tail) to the operating wavelength. Therefore it is important in the development of new chromophores to develop strategies that increase $\beta_{zzz}(\omega,\varepsilon)$ but do not bathochromically shift λ_{max}. Accelerated testing of the photostability of several classes of EO materials has revealed that the most important photochemical decay mechanism involves singlet oxygen.[66] A more detailed discussion of photostability, including characterization techniques, is presented in section 5.4.

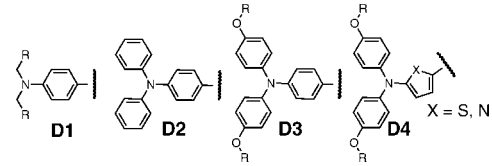

Figure 9. Examples of aryl amine electron density donor structures.

3. Improved Organic EO Materials

3.1. High β Chromophores

Most recently, great interest has been focused around a number of highly successful materials. In particular, arylamine type donors,[67] the tricyanofuran-based (TCF) family of acceptors,[68] and ring-locked tetraene (CLD) or 2,5-divinylthienyl (FTC) bridges have all proven to afford highly active and stable dipolar EO chromophores. This general class of materials has served as the basic π-conjugated building blocks upon which many of the newest molecularly engineered EO materials are based. For this reason, there remains strong continued interest in improving the properties of these materials as well as the synthetic strategies for their preparation. In addition, multidimensional charge transfer (e.g., X-shaped and higher order symmetry),[43,69−72] and twisted intramolecular charge transfer (TICT) chromophores[31,73−76] have been explored as alternative strategies to improve hyperpolarizability or the trade-off between EO activity and optical transparency (r_{33} vs optical loss). Most notably, TICT chromophores have recently been shown to exhibit extremely large nonlinear optical activity.

3.1.1. Electron Donors

A large number of electron density donor groups have been explored over the past decade. The most successful type donor structure falls into the general class of alkyl and aryl amines. In the correct geometry, the energy level of the nitrogen nonbonding lone pair is well matched to donate into the π^* of the attached aromatic ring. This arrangement destabilizes the HOMO and reduces ionization potential creating a strong electron density donating effect.

Figure 9 shows examples of several of the most common aryl amine electron density donor structures. Dialkyl-substituted structures (**D1**) combine strong electron-donating effects with ease of synthesis and secondary functionalization. Simple triaryl amine donors (**D2**) typically display

Scheme 1. Synthesis of the *N*,*N*-bis-(4-methoxyphenyl)-amino-pyrrole donor-aldehyde D4a[a]

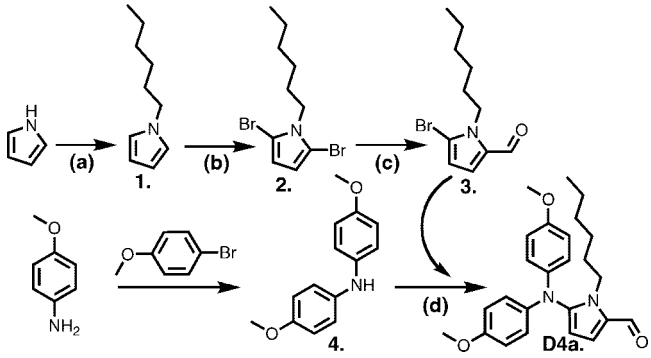

[a] Reagents and conditions: (a) 1-bromo-hexane, NaH, THF, 65 °C, 12 h; (b) NBS, THF, −78 to −15 °C, 4 h; (c) *n*-BuLi, THF, −78 °C, 1 h, then DMF, rt, 1 day; (d) 2 mol % $Pd_2(dba)_3$, 4 mol % $(t\text{-Bu})_3P$, *t*-BuONa, toluene, reflux, 18 h.

reduced hyperpolarizabilities due to stabilization of the nitrogen lone pair, lower solubility, and less synthetic versatility. However, triaryl amine donors display much greater thermal stability than the alkyl analogues. Hyperpolarizability may be improved while maintaining high stability through the introduction of various alkoxy substituents (**D3**).[77−80] Such modification also introduces sites that may be functionalized in order to improve solubility and other characteristics. Another type of triaryl amine donor (**D4**) replaces the phenyl ring that is directly conjugated with the bridge with a heteroatomic aromatic ring such as thiophene or pyrrole. In this case, reduced aromatic stabilization contributes to increased donating strength.[37,81−83] Similar examples exist in which dialkylamino-heteroaryl donors were explored.[84−86]

While starting materials for the simple dialkyl aryl amine donors exemplified by structures **D1** and **D2** are largely commercially available at a reasonable cost, structures **D3** and **D4** require a number of synthetic steps. These synthetic preparations typically proceed through Hartwig−Buchwald-type palladium-catalyzed aryl halide amination chemistry. In the case of **D3**, *N*,*N*-bis-(4-methoxyphenyl)amine was first prepared through this general metal-catalyzed cross-coupling methodology. The amine was then coupled, through a second Hartwig−Buchwald reaction, with 4-bromobenzonitrile, followed by DIBAL-H reduction, to yield the phenyl analog of **5a** in 73% overall yield.[79] A revised approach eliminates the reduction step by directly coupling the amine with 4-bromo-aryl aldehyde, reducing the number of synthetic steps and increasing the overall yield to 89%.[37]

Shown in Scheme 1, the synthesis of the *N*,*N*-bis-(4-methoxyphenyl)-amino-pyrrole donor-aldehyde **D4a** was somewhat more complicated. This synthesis required dibromination and formylation of 1-hexyl-1*H*-pyrrole to yield the starting material **3** for the preparation of **5a** in 59% overall yield.[37]

3.1.2. Electron Acceptors

Like electron-donating substituents, a large number of electron density acceptor groups with diverse chemical structures have been prepared and tested over the past decade. Recently, the majority of research efforts have focused on the 2-(3-cyano-4,5,5-trimethyl-5*H*-furan-2-ylidene)-malonitrile (TCF) and 2-dicyanomethylene-3-cyano-4,5-dimethyl-5-trifluoromethyl-2,5-dihydrofuran (CF_3-TCF) family of acceptors. This acceptor class combines high chemical, thermal, and photostability with strong electron affinity. Following the success of materials based on the unfunctionalized TCF acceptor,[87] significant effort has been focused toward chemical modifications that improve electron affinity, allow secondary functionalization, or modify chromophore shape.

Several modified TCF structures are shown in Figure 10. Simple TCF (**A1**) is illustrated for comparison. Several modifications were reported in which either the 3-cyano or the 2-dicyanomethylene group was replaced by alternate electron accepting moieties such as thiobarbituric acid (**A2**).[88] Efficient synthetic schemes were also developed by which modification of the 5,5-dimethyl group could be accomplished to include attachment points (**A3**)[89] or additional electron-withdrawing substituents.[90−93] Modification of the 5,5-dimethyl positions to include a trifluoromethyl yielded the 2-dicyanomethylene-3-cyano-4,5-dimethyl-5-trifluoromethyl-2,5-dihydrofuran (CF_3-TCF) acceptor. Addition of the CF_3 group has proven to be the most significant improvement in the TCF acceptor class to date. In the case of simple chromophores, switching from TCF to CF_3-TCF may reduce the optical bandgap ΔE_{ge} by as much as 0.3−0.5 eV and roughly double $\beta_{zzz}(\omega,\varepsilon)$.

TCF **A1** may be prepared through standard thermal methods by reacting the α-hydroxy ketone with 2 equiv of malononitrile in the presence of a base under dehydrating conditions.[68] The reaction proceeds by condensation with 1 equiv of malononitrile followed by intramolecular cyclization. The imine intermediate then condenses with a second equivalent of malononitrile to afford the TCF structure in reasonable yield. However, when the α-hydroxy ketone precursor was substantially modified, the yield of the final acceptor fell precipitously.[90] In the case of CF_3-TCF, the yield fell to approximately 25%. Through the use of focused microwave-assisted synthesis methods, the synthetic yields of both simple TCF and CF_3-TCF were improved to 88% and 55%, respectively.[88,94]

The general synthesis of TCF derivatives using focused microwave-assisted synthesis is presented in Scheme 2. The imine intermediate (**2**) may be isolated if the reactant ratio is limited to 1 equiv of malononitrile. This intermediate may then be further reacted with other active methylene groups such as thiobarbituric acid (**A2**) through a Knoevenagel-type condensation. Synthesis of acceptors **A3**−**A6** begins with 2,2,2-trifluoroacetone or the appropriately substituted 2,2,2-trifluoroacetophenone (**3**). Lithiated ethyl vinyl ether is then introduced to yield intermediate **4,** which is deprotected under acidic conditions producing the corresponding fluorinated α-hydroxy ketone. The α-trifluoromethyl ketone is then condensed with malononitrile to yield the substituted acceptor.

3.1.3. Bridges and Chromophores

Aromatic, thiophene-based FTC[95,96] bridges serve as a particularly convenient platform for synthetic modification aimed toward tuning intermolecular interactions because they offer an attractive compromise between large $\beta_{zzz}(\omega,\varepsilon)$ and stability under a wide range of chemical synthesis conditions. When an aromatic bridge unit is employed, chromophore stability is typically improved, but hyperpolarizability is reduced compared with the use of a polyene bridge. The aromaticity of the ring lowers the HOMO energy, lessening the susceptibility of the material to oxidation and chemical reaction. This stabilization also increases the resistance of

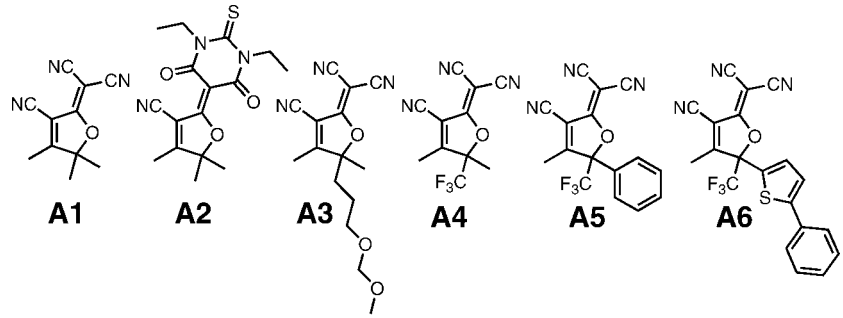

Figure 10. Chemical structures of electron acceptors belonging to the general TCF class.

Scheme 2. Synthesis of Substituted TCF Acceptor Derivatives[a]

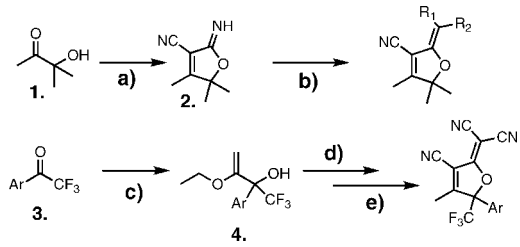

[a] Reagents and conditions: (a) NaOEt, EtOH, malononitrile, microwave, 8 min (76%); (b) NaOEt, EtOH, (R_1 or R_2), microwave, 8 min; (c) ethyl vinyl ether, *t*-BuLi, −78 °C; (d) HCl; (e) NaOEt, EtOH, malononitrile, microwave, 1 h.

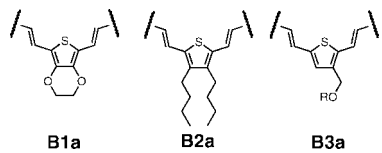

Figure 11. Modifications of the thiophene-based bridging unit for use in EO chromophore synthesis.

the ring to electronic polarization. Analogous to donor design, in order to combat this effect, thienyl rather than phenyl rings are used in the chromophore bridge because of the reduced aromaticity of the heteroatomic ring.[50,97,98] Additionally, chromophore bridge structures based on ethylenedioxythiophene (EDOT), propylene dioxythiophene (PRODOT), bis-EDOT, bis-PRODOT, and bithiophenes have been reported (**B1a**, Figure 11).[99−102]

Many modifications of the simple thienyl-vinylene structure have also been explored for enhanced solubility (**B2a**)[95] and the addition of attachment points (**B3a**) for further structural modification.[103−105] Combining the modified triaryl amine *N*, *N*-bis-(4-methoxyphenyl)aryl-amino donors with the CF_3-TCF acceptors has been shown to lead to chromophores with extremely high $\beta_{zzz}(\omega,\varepsilon)$. For example, the chemical structures of three *N*,*N*-bis-(4-methoxyphenyl)aryl-amino donor based FTC chromophores are shown in Figure 12 (left) along with their corresponding UV−visible absorption spectra (right). The absorption spectra clearly show a pronounced bathochromic shift in $\lambda_{max}(\omega_{eg})$ as the donor aryl ring is changed from phenyl to thiophene and finally to pyrrole. For these materials, DFT quantum mechanical analysis coupled with the two-state model TSM approximation predicted a zero-frequency hyperpolarizability ($\beta_{zzz}(0)$) enhancement of approximately 2-fold upon donor modification from dialkyl-amino (YLD_156) to diaryl-amino regardless of the identity of the third aryl ring. However, when frequency dependence and relative poling induced order were taken into account using the TLM approximation and variable angle polarized absorption spectroscopy (VAPAS), respectively, it was shown that DFT correctly predicted the 3-fold enhancement in r_{33} observed experimentally within the chromophore series.[37] Simple guest−host preparations containing these materials yielded EO coefficient values of r_{33} = 110 pm/V {ATR λ_{exp} = 1.33 μm}, measured using the attenuated total reflection (ATR) technique. These data represent a 3-fold improvement in EO coefficient over chromophores composed of the same thienyl-vinylene bridge and CF_3-TCF acceptor.

The synthetic preparation of chromophores **A**−**C** here serves to exemplify typical methods for the synthetic preparation of EO materials containing thiophene-based bridges (Scheme 3). The use of high yielding and versatile Horner−Wadsworth−Emmons olefination and Knoevenagel condensation chemistries to create the EO chromophore conjugated backbone is typical of modern chromophore synthesis. Chromophore synthesis began with the preparation of the donor unit **D4**. Following the successful synthesis of the *N*,*N*-bis-(4-methoxyphenyl)aryl-amino donor units, preparation of the complete chromophores **A**−**C** was straightforward and proceeded in high yield. Horner−Wadsworth−Emmons olefination chemistry was used to couple donor and bridge yielding **DB1**, which was then formylated to yield **DB2**. The CF_3-phenyl TCF acceptor (**A5**) was then introduced via Claisen−Schmidt condensation conditions in anhydrous ethanol. The overall yields of **A**, **B**, and **C**, were 51%, 19%, and 34%, respectively.

Because of approximately a factor of 2 increase in $\beta_{zzz}(\omega,\varepsilon)$, when compared with the thiophene bridge, optimization of polyene (e.g., tetraene) bridge-based chromophores has also been the subject of considerable research effort (CLD).[12,87,104,105] However, some of the newest versions of tetraene bridge-based chromophores (incorporating CF_3-TCF acceptor) are less chemically, thermally, and photostable than the thiophene analogs. Reduced chemical stability has limited the range of secondary structures (dendrimers, side-chain polymers) synthesized incorporating the tetraenes. Therefore, much recent research effort has been focused toward improving stability and overall utility. Donor modification has led to thermal stability up to 330 °C using the simple TCF acceptor[78,80] and up to 237 °C using CF_3-TCF, while retaining excellent EO properties.[79]

To address chemical and photostability, bridge modification through substitution of the 2-position of the isophorone ring has been explored. These schemes have included alkyl substitution,[106] alkoxy substitution,[107] and thiolation.[108] Several thiolated tetraene chromophores (chromophore **1**) were synthesized and compared against the analogous unfunctionalized chromophore (chromophore **2**) (Figure 13). When irradiated in solution in the presence of a singlet oxygen generator (methylene blue), chromophore **1** revealed pho-

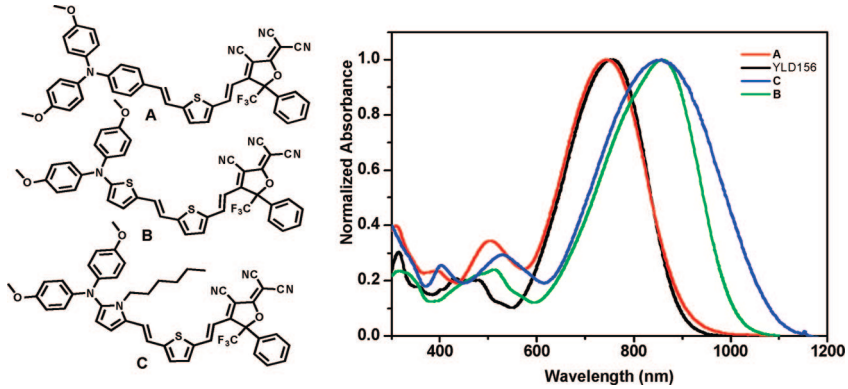

Figure 12. Chemical structures (left) of *N*,*N*-bis-(4-methoxyphenyl)aryl-amino donor based FTC chromophores and normalized UV−visible absorption spectra (right) of chromophores **A**−**C** compared with that of YLD_156. Reprinted with permission from ref 37. Copyright 2008 American Chemical Society.

Scheme 3. Synthesis of Completed *N*,*N*-bis-(4-methoxyphenyl)aryl-amino donor chromophores A−C[a]

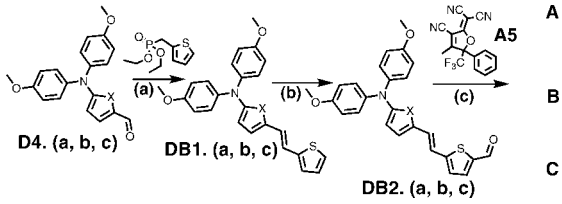

[a] Reagents and conditions: (a) *t*-BuOK, THF, 0 °C to rt, 8 h; (b) *n*-BuLi, THF, −78 °C, 1 h, then DMF, rt, 1 day; (c) CF_3Ph−TCF acceptor, EtOH, 8 h rt.

tostability enhanced by approximately an order of magnitude in comparison to chromophore **2**. Additionally, $\beta_{zzz}(\omega,\varepsilon)$ was improved by 34% ($\beta_{HRS}(2\omega,\varepsilon) = 10\,200 \times 10^{-30}$ esu {HRS $\lambda_{exp} = 1.907$ μm), EO coefficient was improved by 38% ($r_{33} = 219$ pm/V {Teng−Man $\lambda_{exp} = 1.33$ μm}under a poling field of $E_p = 120$ V/μm), and the optical absorption maximum was hypsochromically shifted by 17 nm.

Although the best results were obtained using the thiolate-bridge chromophores, chemical stability (particularly toward the Diels−Alder cross-linking reaction) and photostability were also improved in the alkyl- and alkoxy-substituted materials. In the case of the thiolated materials, the hypsochromically shifted in λ_{max} may be understood in terms of Dewar's rules stating that substitution at the position indicated with an electronegative sulfur atom should indeed alter the electronic properties in this manner.[108,109] The observed increased resistance to singlet oxygen and improved chemical and photostability that seems to be a general feature of the substituted-isophorone polyenes can be largely attributed to the protection of the otherwise labile proton from chemical reaction. Such substitution also serves to force the bridge into an all-trans configuration reducing the potential for Diels−Alder diene-like behavior (cis configuration),[107] and improving hyperpolarizability.[106]

Synthesis of the thiolated polyene chromophores (Scheme 4) began with preparation of epoxyisophorone followed by nucleophilic substitution with the alkanethiol, affording the thiol-substituted isophorone **5** in nearly quantitative yield. Base-catalyzed Claisen−Schmidt condensation of **5** with the donor aldehyde yielded donor-bridge **9**. Horner−Emmons olefination followed by DIBAL-H reduction and further acceptor condensation completed the synthesis in 33% yield over the last four steps.

X-shaped chromophores represent multidimensional charge-transfer conjugated π-electron systems in which the dipole vector is oriented between the two arms of the X. These systems exhibit significantly hypsochromically shifted absorption maxima due to excitonic coupling between the transition dipoles of the two molecular charge transfer components.[110] Despite the blue-shifted λ_{max}, hyperpolarizability is enhanced relative to the one-dimensional structural analog. In this type of π-system, hyperpolarizability and λ_{max} are predicted to depend strongly on substitution arrangement.[43] X-shaped chromophores also present the advantage of improved geometry for use in sequential synthesis based self-assembly schemes for direct solution deposition of ordered thin films. In the study cited here, the hyperpolarizability of the X-shaped chromophore (Figure 14) was determined by hyper-Rayleigh scattering as $\beta_{zzz}(2\omega,\varepsilon) = 1840 \times 10^{-30}$ esu {HRS $\lambda_{exp} = 800$ nm}, and film EO coefficient was estimated as $r_{33} \approx 45$ pm/V {$\lambda_{exp} = 1310$ nm} from polarized angle-dependent second harmonic generation (SHG).[69]

Twisted intramolecular charge transfer (TICT) chromophores consist of a conjugated donor−bridge−acceptor π-electron system that contains a rotation about the charge-transfer axis. The degree of rotation has been theoretically predicted to modulate the π-orbital overlap in such a way that electric field induced nonlinear polarization is maximized at an optimum dihedral angle of $\theta \approx 70°-85°$.[111] TICT chromophores reported so far consist of substituted biaryl compounds characterized by charge-separated ground states (Figure 15). The product of hyperpolarizability and dipole moment for molecule **TMC-3** was measured as $\mu\beta = -488\,000 \times 10^{-48}$ esu {EFISH $\lambda_{exp} = 1.907$ μm} using the electric field induced second harmonic generation method (EFISH). Compared with $\mu\beta = 35\,000 \times 10^{-48}$ esu {EFISH $\lambda_{exp} = 1.907$ μm} measured for CLD, this value is extremely large. **TMC-3** possesses a ground-state dipole moment as large as 50.6 D (calculated by DFT methods). This large dipole moment, coupled with the reduced solubility typically displayed by charge-separated (zwitterionic) ground-state chromophores, causes this type of chromophore to aggregate aggressively. Care must therefore be taken in preparing EO materials containing TICT chromophores by choosing an appropriate host or by synthetic modification of the TICT molecule itself to reduce aggregation. When poled in a polar polyvinylphenol host, EO coefficient values of $r_{33} = 330$ pm/V {Teng−Man $\lambda_{exp} = 1.33$ μm} were measured using the Teng−Man technique under an applied poling field of $E_p = 100$ V/μm.[74] It important to note that in the case of

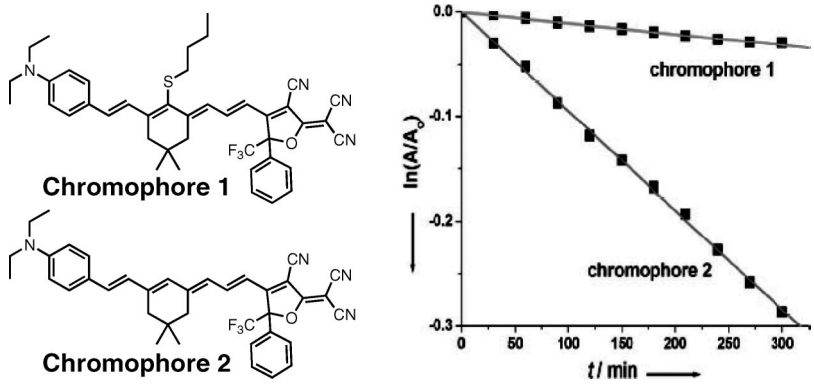

Figure 13. Demonstration of the enhanced photostability of thiolated chromophore **1** compared with unfunctionalized chromophore **2** when irradiated in the presence of a singlet oxygen generator. Reprinted with permission from ref 108. Copyright 2008 American Chemical Society.

Scheme 4. Synthesis of Thiolated Polyene Chromophores 1−3[a]

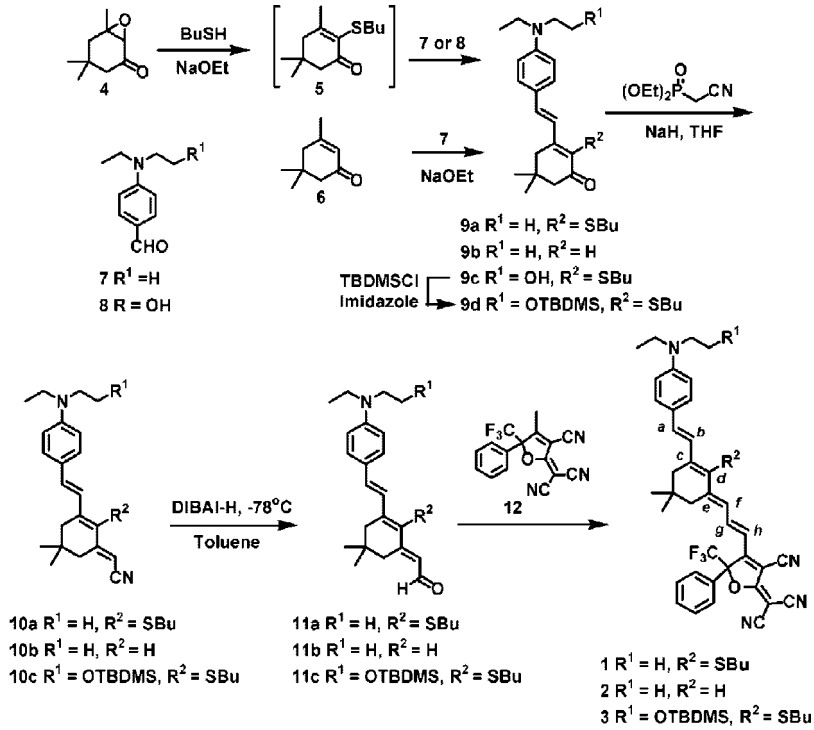

[a] Reprinted with permission from ref 108. Copyright 2008 American Chemical Society.

TMC-3, this extraordinarily high r_{33} value has so far only been measured by *in situ* (constant poling bias) methods.

Synthesis of the extended TICT chromophores began with the preparation of twisted π-system biaryl **5** through Suzuki coupling of the appropriate aryl bromide and boronic acid.[112] Scheme 5 outlines the following synthetic preparation of twisted π-system biaryl halide **6c**. Following deprotection and conversion of **5** to triflate **6a**, a palladium-catalyzed Buchwald−Hartwig amination yielded the diphenyl ketimine derivative **9**. Hydrolysis to amine **10** and subsequent conversion to halide **6c** then followed. Synthesis of the extended TICT chromophores was then completed using palladium-catalyzed Heck-type cross-coupling methodology (Scheme 6). The final synthetic steps were similar for the **TM** and **TMC** series chromophores, including **TMC-3**.

3.2. Molecularly Engineered Materials

With the goal of improved poling efficiency, thermal stability, material compatibility, and synthetic ease, a wide variety of side-chain and main-chain chromophore-substituted polymers have been explored. Due to the availability of a recent review[112] and in the interest of brevity, this review is limited to discussion of recent demonstrations of molecular-level EO material engineering according to the concepts of shape engineering, chromophore site isolation, and active interaction engineering.

3.2.1. Shape Engineering and Site Isolation

Chromophore and material design at the molecular level must not only consider $\beta_{zzz}(\omega,\varepsilon)$ but must also consider how chromophore substitution impacts intermolecular interactions. In a typical guest−host composite material, increasing N beyond the optimum level leads to increased dipole−dipole interaction strength. Stronger interchromophore dipolar interactions cause not only diminished poling induced $\langle\cos^3\theta\rangle$, but also increased optical loss due to guest/host phase separation and increased material inhomogeneity. Therefore, reduction of, or control over, the electrostatic interactions

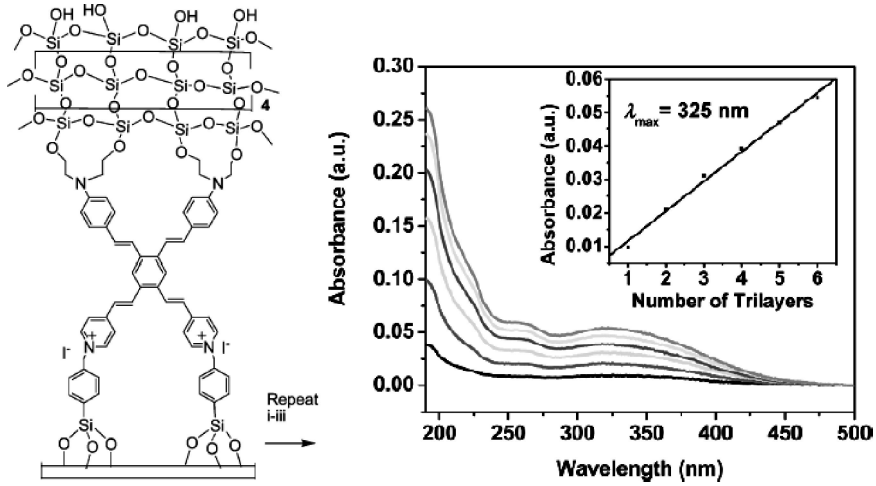

Figure 14. Schematic (left) of a film prepared by sequential synthesis self-assembly of X-shaped chromophores and UV−visible absorption spectrum (right) as a function of layer deposition. Reprinted with permission from ref 110. Copyright 2004 American Chemical Society.

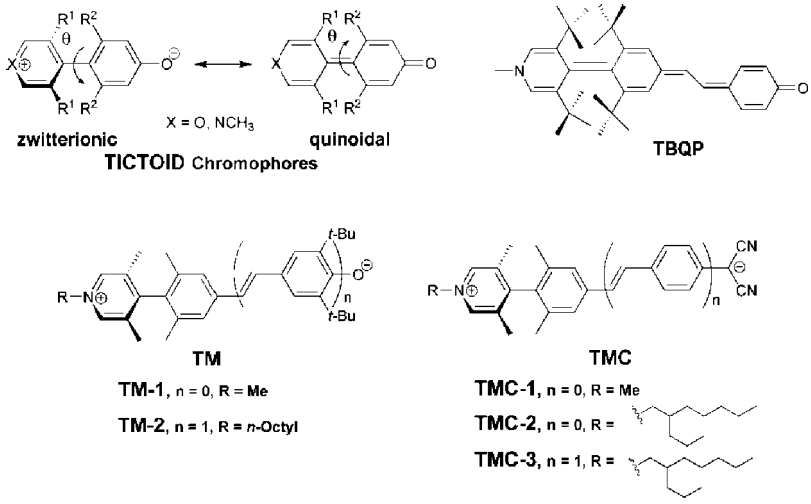

Figure 15. TICT and substituted TICT chromophore structures. Reprinted with permission from ref 74. Copyright 2007 American Chemical Society.

among chromophores not only improves poling efficiency but also enhances compatibility between guest and host, reducing chromophore aggregation, and leading to a more homogeneous material with reduced optical loss. The concepts of shape engineering and site isolation include the modification of individual chromophores (functionalized/dendronized chromophores),[89,102,105,113] multichromophore dendrimers,[36,89,114−118] dendronized polymers,[89,92,119−122] and hyperbranched polymers,[123−125] in order to minimize unwanted dipole−dipole interactions.

Dendrimers or otherwise dendritic structures are well suited to effect molecular architectural control. Steric forces between chromophore substituents may be harnessed to inhibit detrimental side-to-side intermolecular electrostatic interactions. Additionally, statistical mechanical modeling predicts that a spherical molecular shape is ideal in order to optimize $N\langle\cos^3\theta\rangle$, leading to maximum $r_{33}(\omega)$. Because dendrimers are constructed from the successive addition of discrete dendritic units (dendrons), molecular size, shape, and substitution geometry can be controlled with a high degree of precision. Dipolar EO chromophores can be easily incorporated into dendritic structures or functionalized with dendrons in order to create a pseudospherical structure isolating the dipolar unit from its surroundings. Several material concepts have been demonstrated very successfully to date following this design paradigm. A number of these materials have yielded EO coefficients among the highest reported thus far.

In one report, individual chromophores that were prepared specifically to include secondary attachment functionality were modified with dendrons to create dendronized chromophores of pseudospherical shape.[105,113] When dendronized chromophore **7** (Figure 16) was loaded into a poly(bisphenol A carbonate-*co*-4,4′-(3,3,5-trimethyl-cyclohexylidene)diphenol carbonate (APC) host at 12% active chromophore weight and poled at E_p = 100 V/μm, the EO coefficient was measured to be r_{33} = 30 pm/V {Teng−Man λ_{exp} = 1.33 μm} under optimized conditions. Treating undendronized chromophore **6** in a comparable manner, r_{33} = 10 pm/V. The observed 3-fold increase in r_{33} suggests that dendronization greatly facilitates poling response. Dendronized chromophore **7** also displayed λ_{max} = 574 nm (blue-shifted by 29 nm compared with **6** (λ_{max} = 603 nm) when measured in 1,4-dioxane), suggesting that the local environment of the chomophore was indeed significantly altered by dendritic encapsulation. In addition, the optical loss of the composition of **7** in APC was measured by the Lockheed−Martin Corporation to be as low as 0.65 dB/cm {λ_{exp} = 1.5 μm} and 0.85 dB/cm {λ_{exp} = 1.3 μm} using photothermal deflection spectroscopy (PDS).[113]

Scheme 5. Synthesis of Twisted π-System Biaryl Halide 6c[a]

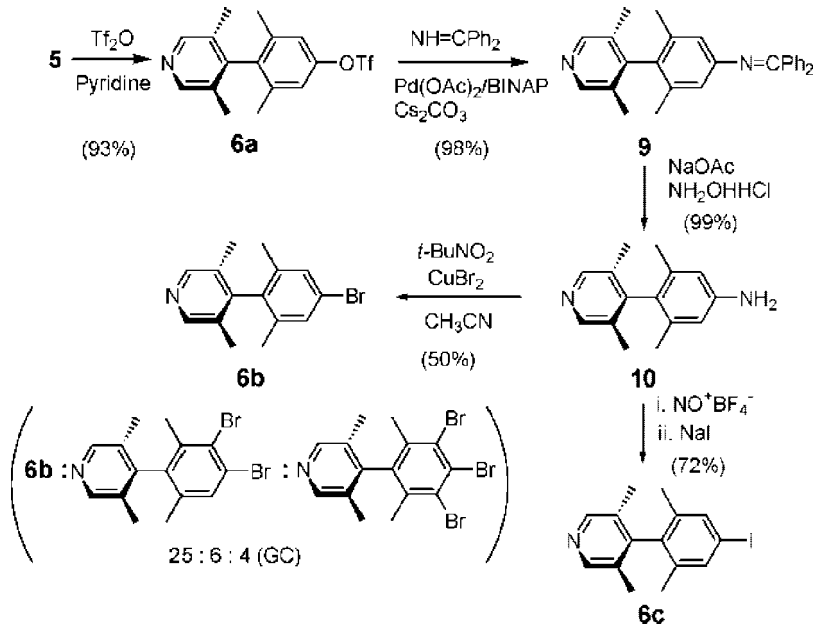

[a] Reprinted with permission from ref 112. Copyright 2005 American Chemical Society.

Scheme 6. Preparation of TM-type TICT Chromophores through Palladium-Catalyzed Heck-type Cross-Coupling Methodology[a]

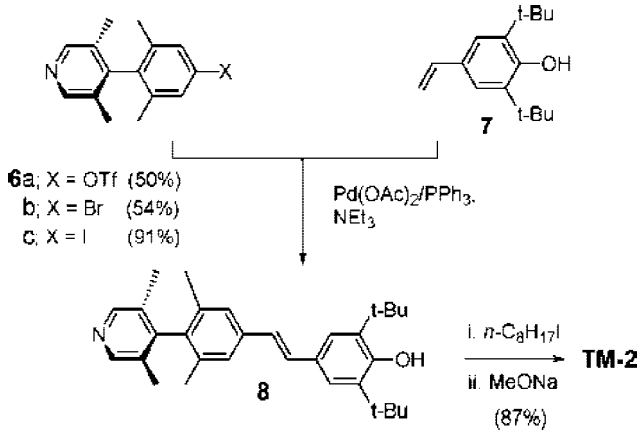

[a] Reprinted with permission from ref 112. Copyright 2005 American Chemical Society.

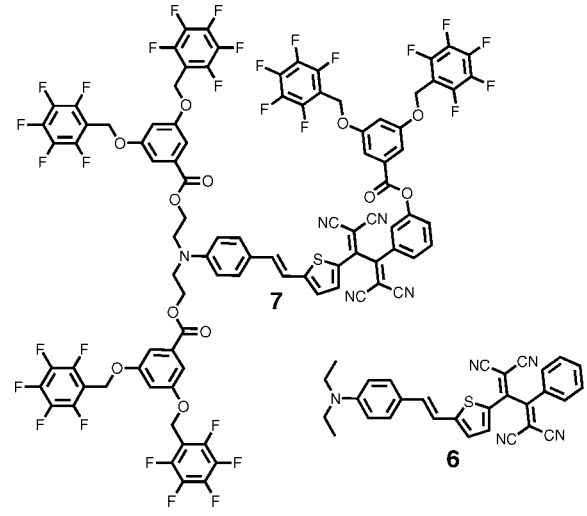

Figure 16. Chemical structures of dendronized chromophore **7** and nondendritic analog **6**. Reference 113 (http://dx.doi.org/10.1039/b200851c)—Reproduced by permission of The Royal Society of Chemistry.

Further demonstration of improved poling efficiency in dendronized materials compared with analogous unfunctionalized chromophores has been realized through the preparation of more chemically elaborate multichromophore dendrimers.[114−116,126] Multichromophore dendrimers consist of large branching structures in which the chromophore units are covalently attached within the void created by the outer periphery. The chromophores are attached in such a way that they are free to rotate but are significantly isolated from one another by the dendrimer core (Figure 17).

The effects of specific attachment geometries have been studied in detail, and the results suggest that attachment geometry is not highly important as long as the chromophore rotation can be significantly decoupled from the dendrimer scaffold. This decoupling is largely dependent on the length of the chromophore-to-core tether and introduces a trade-off between lowered T_g and increased poling efficiency.[117] Unlike the dendronized chromophores, which are loaded as guests into inert polymer hosts, the larger molecular weights (MW) and inherent amorphous nature of the multichromophore dendrimers have allowed many of them to be cast into high optical quality, neat (dendrimer only) photonic thin films. These highly homogeneous dendrimer-based amorphous organic glasses were then poled and analyzed using standard methods.

Data from pseudoatomistic Monte Carlo (PAMC) computer simulations of r_{33}/E_p corresponding to multichromophore dendrimers **41** and **33** is compared with experimental data in Figure 18. The two highest experimental values (solid circles) of N correspond to the inherent number density, as governed by chemical structure, of **41** and **33**. The two lowest values correspond to **33** loaded into APC. Theoretical values assume the best-fit value of $\beta_{zzz}(\omega,\varepsilon) = 3200 \times 10^{-30}$ esu. From inspection of Figure 18, it is apparent that r_{33}/E_p exhibits an approximately linear relationship with N that holds up to the highest value examined (pure **33**). This suggests that the dependence of $\langle\cos^3\theta\rangle$ on N is

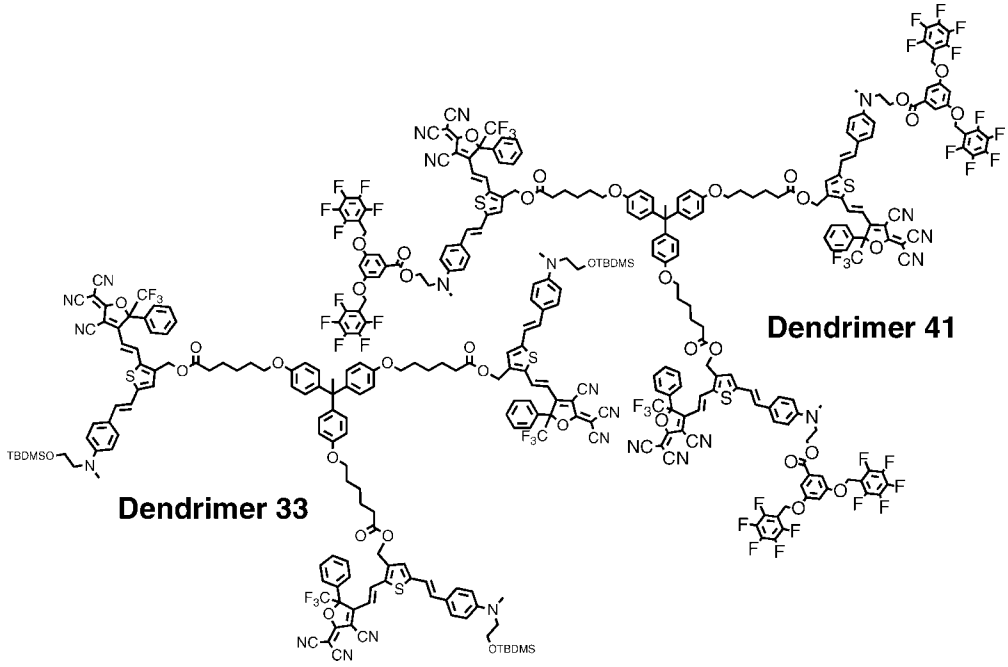

Figure 17. Chemical structure of three-arm multichromophore dendrimers **41** and **33**. Reprinted with permission from ref 36. Copyright 2007 American Chemical Society.

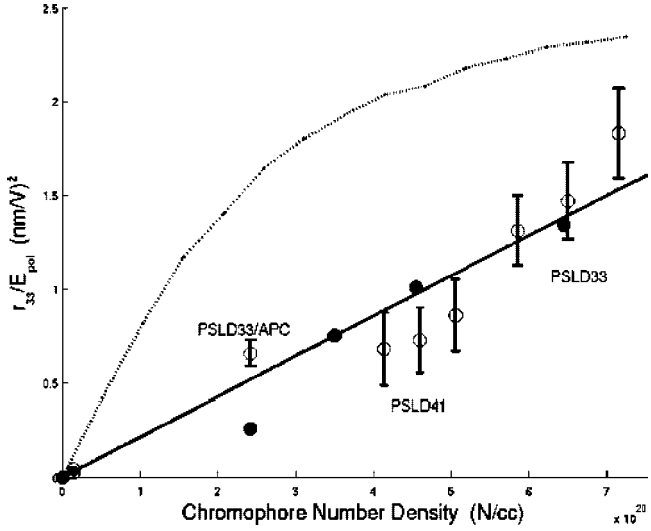

Figure 18. Monte Carlo (MC) statistical mechanical computer simulations of r_{33}/E_p for dendrimers **33** and **41** compared with experimental data as a function of chromophore number density. Open circles represent MC modeling results using several different density settings and assuming a $\beta_{zzz}(\omega,\varepsilon) = 3200 \times 10^{-30}$ esu. Solid circles represent experimental data corresponding to the neat films of dendrimers **41** and **33**, in addition to two measurements in which dendrimer **33** was poled doped into APC at varying concentrations. Reprinted with permission from ref 36. Copyright 2007 American Chemical Society.

greatly diminished in the case of the dendrimers. For simple chromophores in a polymer host, the EO roll-off behavior begins to occur at $N \approx (1.5-2.5) \times 10^{20}$ molecule/cm^3[34] and for dendrimer **33** at $N = 6.5 \times 10^{20}$ molecule/cm^3.

The synthesis of multichromophore dendrimers (Scheme 7) is generally straightforward, beginning with relatively standard EO chromophore preparation.[36] After chromophore preparation, the chromophore is attached to the core, and the outer periphery is finally introduced in a somewhat convergent manner. Examples also exist in which the dendrimer was prepared linearly, including chromophore synthesis, starting from the multiarm core structure.[114] One

Scheme 7. Synthesis of Multichromophore Dendrimers 33 and 41[a]

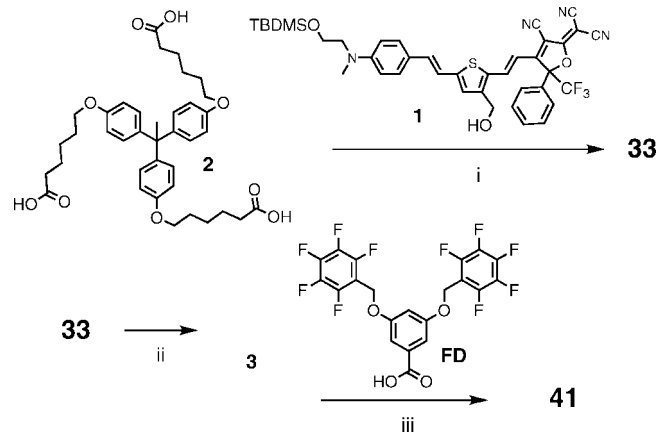

[a] Conditions: (i) DCC/DPTS, DCM/DMF, reflux 48 h, 50%; (ii) 1 N HCl (MeOH soln), acetone, rt 2.5 h, quant.; (iii) DCC/DPTS, DCM/DMF, reflux 48 h, 62%. Reprinted with permission from reference.[36] Copyright 2007 American Chemical Society.

of the drawbacks of neat multichromophore dendrimer films is that their T_g is usually significantly lower than that of high molecular weight polymeric EO materials requiring extensive use of cross-linking chemistries in order impart acceptable r_{33} temporal stability at elevated temperatures.[105,115,118]

Hyperbranched polymer EO materials (HPEOs) represent a site-isolation concept that is closely related to multichromophore dendrimers. However, unlike the monodisperse dendrimers, HPEOs are inherently more random in structure and polydisperse. Such systems are therefore expected to exhibit more batch-to-batch property variability, but synthetic preparation may be facilitated. HPEOs are usually of relatively low molecular weight (although typically larger than dendrimers) and generally also require extensive cross-linking to achieve high thermal stability (T_g > 150 °C). A number of examples of hyperbranched polymers with varying properties have been prepared and studied.[124,125]

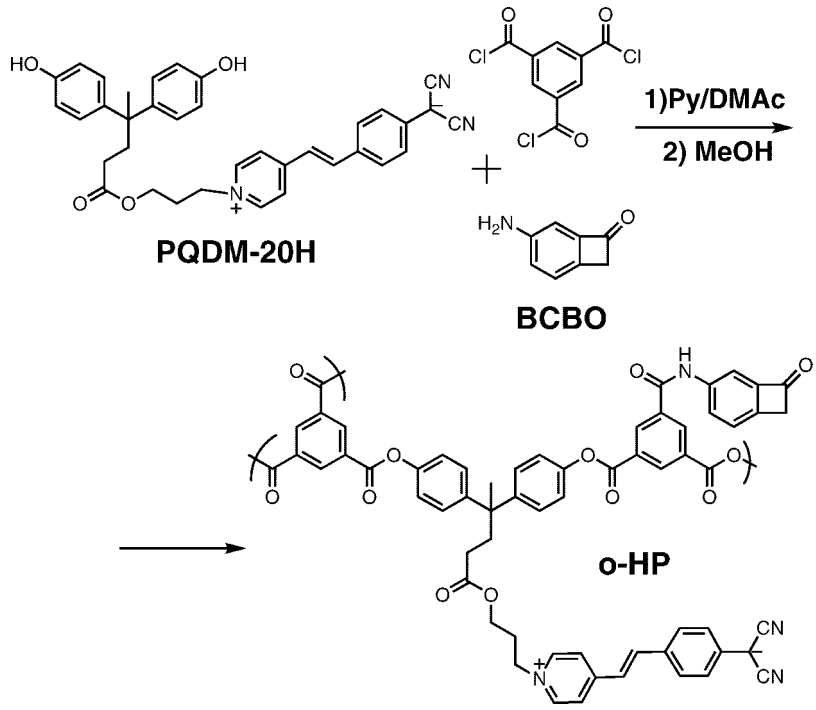

Figure 19. Hyperbranched NLO oligomer prepared as a macromolecular dopant.[123]

A very interesting approach to HPEOs is illustrated in Figure 19. In this study, hyperbranched oligomers (o-HP) (containing a zwitterionic ground-state pyridinium tricyanoquinonedimethane (PQDM) chromophore) were prepared as a macromolecular dopant. The PQDM chromophore is reported to deliver a quite high $\beta_{HRS}(2\omega,\varepsilon) = 1930 \times 10^{-30}$ esu {HRS $\lambda_{exp} = 1.07$ μm} value. The o-HP oligomer also contained a 5-aminobenzocyclobutenone (BCBO) unit that underwent a ring-opening followed by a dimerization (cross-linking) reaction at temperatures above 200 °C. Mixtures of 15% by weight o-HP dispersed into a high T_g poly(ether sulfone) were poled at 170−190 °C under a poling voltage of $E_p = 70-90$ V/μm followed by heating at 200 °C. The resulting EO coefficient was measured as $r_{33} = 65$ pm/V {Teng−Man $\lambda_{exp} = 1.55$ μm} and retained 90% activity after annealing at 85 °C for more than 1200 h.[123]

Dendronized polymers were developed in order to reduce synthetic expense, improve device processing related issues (material compatibility, film forming, and mechanical properties), and increase thermal stability compared with dendrimers and HPEOs. The site-isolation effect in dendronized polymers relies on either affixing a dendron-functionalized chromophore to a polymer backbone[121,122,126] or attaching a bulky dendron to the polymer backbone directly, placed between the side-chain chromophores.[92,126]

Several very elegant demonstrations of dendronized polymers have been reported using Diels−Alder "click" chemistry-based postpolymerization functionalization schemes. The example shown in Figure 20 illustrates this methodology used to create a side-chain dendronized polymer that may be further cross-linked during the poling process. In this example, Diels−Alder polymer postfunctionalization with the active dendronized chromophore was performed in solution. The solvent was then removed, varying amounts of bis-maleimide cross-linker (BMI) were added, and the resulting mixture was spin-cast to create thin films. Poling these films under $E_p = 125-160$ V/μm yielded a maximum EO coefficient of $r_{33} = 60$ pm/V {Teng−Man $\lambda_{exp} = 1.33$ μm}, which maintained over 95% activity when tested at 85 °C for 500 h.[119] By simple alteration of the processing conditions, it was discovered that this EO activity could be increased up to $r_{33} = 110$ pm/V {Teng−Man $\lambda_{exp} = 1.33$ μm}. In this case, the free dendronized dienophile chromophore was blended with the diene polymer to create a guest−host mixture. This mixture was then poled, generating the side-chain polymer *in situ*.[120] This processing method allowed for higher chromophore mobility prior to side-chain attachment, resulting in higher poling-induced order. This study also noted that if the chromophore content was increased past the point of saturating the Diels−Alder functional groups present in the polymer, an unanticipated increase in EO coefficient occurred.

Polymer backbones used in the preparation of dendronized polymers have included acrylic polymers (Figure 21),[119] polyesters,[92] polyurethanes,[121] and polyimides.[127,128] Equally diverse examples of postfunctionalization strategies have included Diels−Alder, esterification,[126] 1,3-dipolar addition,[122] and urethane,[127] chemistries. Postpolymerization functionalization schemes have been employed because of the sensitivity of some EO chromophores to polymerization conditions and because of the increased versatility offered by alteration of the EO material composition simply by changing the mixing ratio. In order to be successful, postfunctionalization (and cross-linking) reactions must be extremely high-yielding and mild and ideally produce few or no byproducts.

3.3.2. Active Interaction Engineering; Spatially Anisotropic Interactions

The concept of active interaction engineering encompasses the use of inherently spatially anisotropic intermolecular interactions, such as aryl-fluoroaryl,[93] hydrogen bonding,[129,130] liquid crystalline,[131] molecular chirality,[132] and binary chromophore interactions,[15,54,133] to drive spontaneous or enhanced poling-induced acentric ordering. Secondary elec-

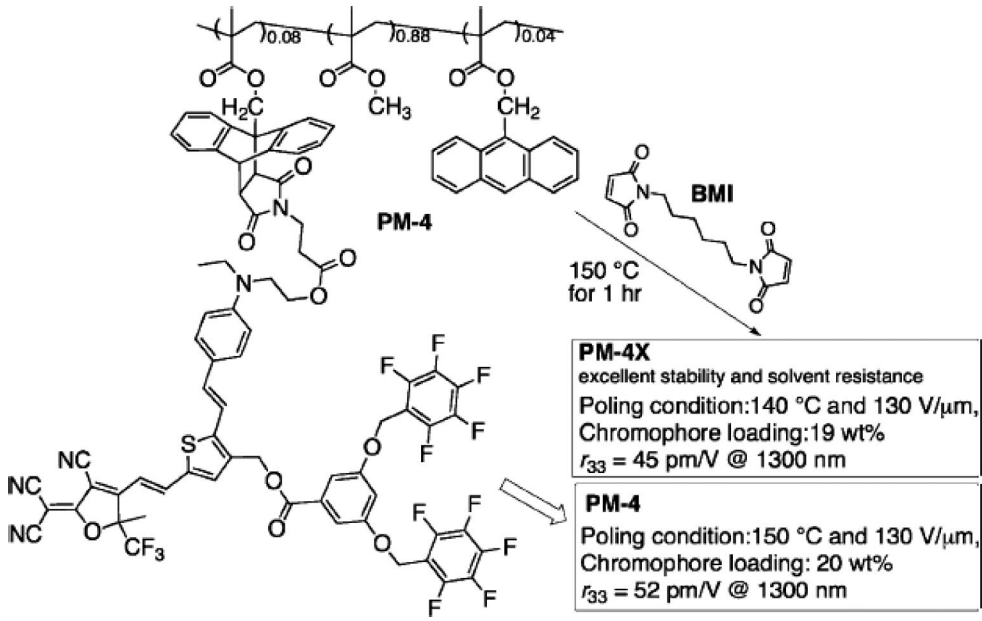

Figure 20. Example of a cross-linkable dendronized EO polymer created by Diels−Alder "click" postfunctionalization of an anthracene (Diels−Alder diene) containing acrylic polymer. Reprinted with permission from ref 119. Copyright 2006 American Chemical Society.

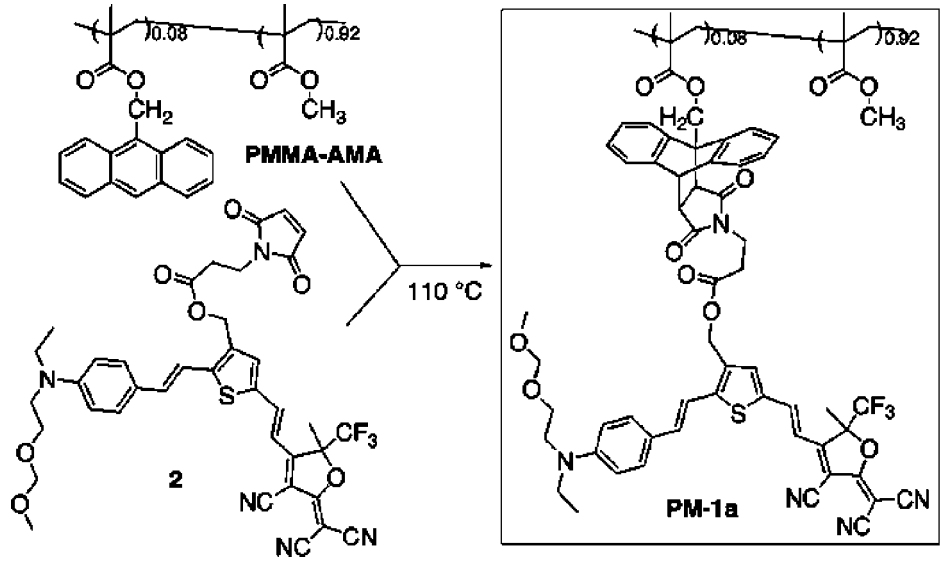

Figure 21. Synthetic preparation of a side-chain dendronized polymer through Diels−Alder "click" chemistry. Reprinted with permission from ref 119. Copyright 2006 American Chemical Society.

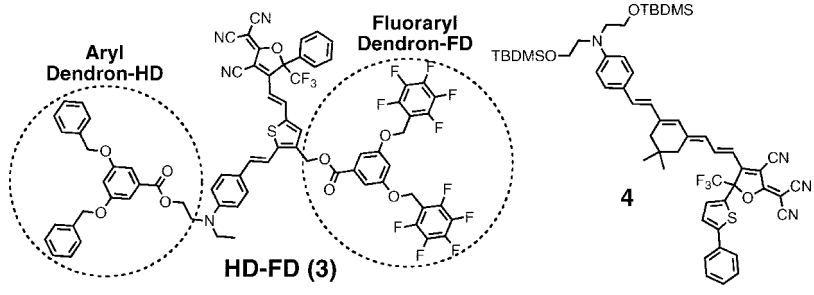

Figure 22. Chemical structure of asymmetrically aryl-dendron- and fluoroaryl-dendron-substituted dendronized chromophore.[93]

trostatic forces may serve to compete against dipole−dipole forces or create lattice structures of reduced dimensionality. In many cases, chromophore functionalization to engineer such active interactions also serves to site-isolate the dipoles and physically attenuate detrimental electrostatic forces.

Introduction of spatially anisotropic aryl−fluoroaryl interactions through asymmetric synthesis methods has been demonstrated to improve both poling efficiency and thermal stability in poled dendronized chromophore films.[93] Figure 22 illustrates asymmetric substitution of an EO chromophore with aryl and fluoroaryl dendrons (**3**). The selective attractive interactions between the electronegative phenyl groups and electropositive pentafluorophenyl groups introduce asymmetric interchromophore interactions that help to stabilize

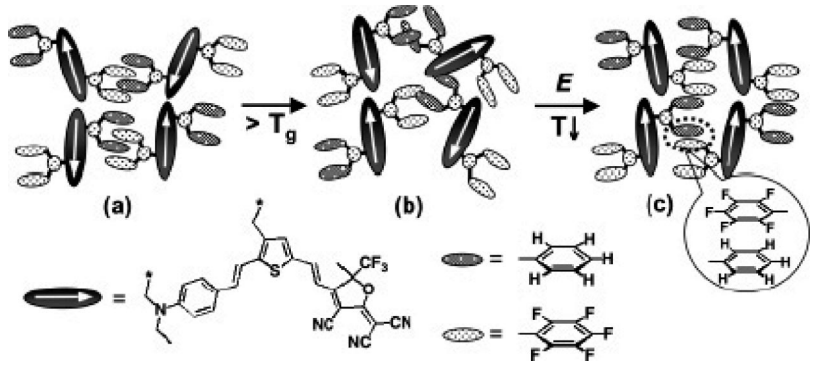

Figure 23. Graphical illustration of the alignment formation of self-assembled chromophores by aryl-fluoroaryl interactions: (a) locked random dipoles (shown as arrows) before poling; (b) unlocked random dipoles before poling (heated); (c) locked acentric dipoles after poling (cooled). Reprinted with permission from ref 93. Copyright 2007 American Chemical Society.

poling-induced order. This concept is graphically illustrated in Figure 23.

The initially random solid (a), composed of **3**, was heated to near T_g in order to dissociate intermolecular interactions (b). A poling field was then applied to introduce acentric dipolar order, followed by cooling of the films with continued application of the poling field (c). As the films cooled, the HD and FD groups reassociated to enhance and stabilize order. By application of this approach, EO coefficients as high as $r_{33} = 108$ pm/V {Teng−Man $\lambda_{exp} = 1.31$ μm}were achieved under $E_p = 100$ V/μm, compared with $r_{33} = 52$ pm/V for the analogous dendronized chromophore without the aryl−fluoroaryl substitution.[93] The concept of binary chromophore organic glasses (BCOG) was also introduced during the course of this study. When chromophore **4** was blended with **3**, unprecedented electro-optic coefficients of $r_{33} = 327$ pm/V {Teng−Man $\lambda_{exp} = 1.31$ μm} under $E_p = 80$ V/μm were realized.

Binary chromophore organic glasses (BCOGs) offer a new design paradigm for organic EO materials in which a second high-$\beta_{zzz}(\omega,\varepsilon)$ EO chromophore is introduced into a chromophore-containing host material (EO dendrimer, side-chain polymer, etc.).[15,53,54,134] Increasing concentrations of the second (guest) chromophore lead to a pronounced increase in electro-optic coefficient. The rate of this enhancement with respect to chromophore number density is approximately linear and is a factor of 2−3 larger than that measured for the same chromophore in a traditional inert polymer host.[53] BCOGs also allow very large chromophore number densities to be used due to improved compatibility between guest and host materials. Phase separation problems that lead to decreased poling efficiency and high optical loss in more traditional materials are reduced. However, very high chromophore number density can lead to increased material conductivity, reducing the maximum E_p that may be applied and limiting r_{33}.

Figure 24 depicts two different BCOGs and illustrates this general enhancement effect. In this study, a tetraene guest chromophore (YLD_124) was doped into a multichromophore dendrimer (a) and a side-chain EO polymer (b). A plot of poling efficiency (r_{33}/E_p), as a function of N (with the host contributions removed) (right) revealed that the rate of increase in r_{33}/E_p was significantly enhanced relative to the similar experiment in which APC was used as the host. This behavior implied that $\beta_{zzz}(\omega,\varepsilon)$, $\langle\cos^3\theta\rangle$, or a combination of the two was improved in the case of BCOGs. Theoretical modeling showing excellent agreement with the experimental data suggested that spatially anisotropic intermolecular electrostatic interactions between guest and host materials resulted in improvements in $\langle\cos^3\theta\rangle$.[54] The existence of a strong coupling between poling-induced guest order and the arrangement of the host lattice was also confirmed by laser-assisted poling (LAP) experiments.[134] These LAP experiments are discussed further in the following sections. Enhanced hyperpolarizability was also expected as a result of the increased dielectric constant of the chromophore-containing host.

In addition to unprecedented r_{33}, the design of BCOGs is also amenable to the incorporation of various cross-linking chemistries. When Diels−Alder-based cross-linking strategies were used, postpoling T_g's of over 200 °C have been realized.[15,135] Binary chromophore materials also display photostability at operational wavelengths ($\lambda_{exp} = 1.55$ μm) that is improved by approximately 1 order of magnitude.[53,66]

4. Materials Processing Methodologies

4.1. Electric Field Poling

Electric field poling has been extensively studied, and several reviews exist covering the topic.[12,26,136−138] For this reason, only a brief overview is presented here. Electric field poling may be performed using a number of experimental configurations. The two most common poling configurations are corona poling and contact electrode poling. Advantages of corona poling include the ability to apply very high poling fields and process large areas. The most critical disadvantage of the corona poling technique is the inherent difficulty in accurate determination (monitoring) of the magnitude of the applied field. Corona poling is performed employing a lower electrode on which the EO thin film is cast and an upper needle or wire electrode or electrode array that is held some distance from the top surface of the EO film.[138]

Unlike corona poling, contact electrode poling employs two electrodes that are in direct contact with the EO material. These electrodes can be oriented in-plane, where the poling axis is parallel to the device surface,[139] or vertically, where the poling axis is normal to the device surface. Vertical orientation is the most common configuration due to ease of device fabrication and compatibility with standard r_{33} measurement techniques. Contact electrode poling has the advantage of much lower working voltages than corona poling and simple measurement of applied voltage and leakage currents. In addition, contact poling electrodes may also be used as the driving electrodes for completed electro-optic devices.

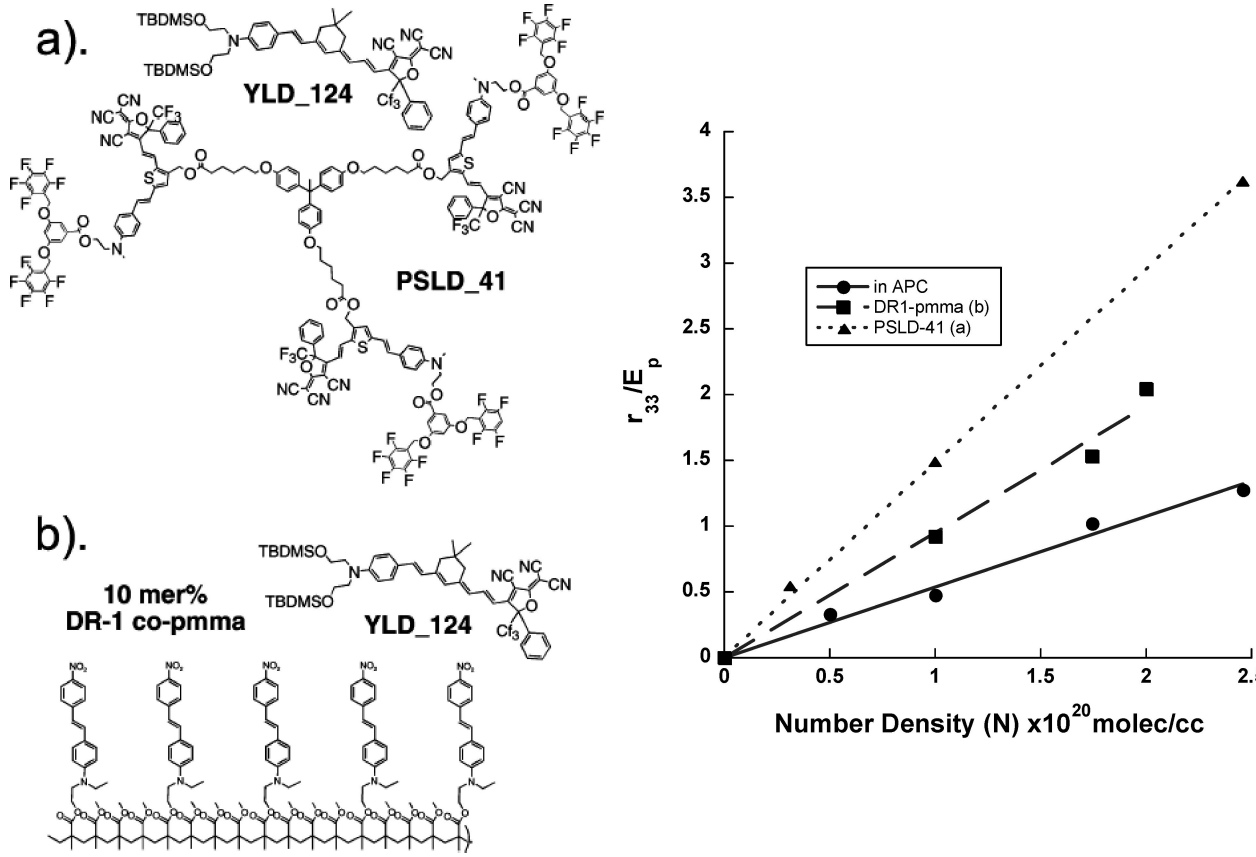

Figure 24. Guest chromophore dopant YLD_124 (left) blended into (a) EO dendrimer PSLD_41 and (b) EO side-chain polymer DR1-*co*-PMMA and poling efficiency (r_{33}/E_p) of YLD_124 (right) poled in the panel a blend (▲) and the panel b blend (■) with host contribution subtracted and in APC (●) for comparison. Reprinted with permission from ref 54. Copyright 2008 American Chemical Society.

In either corona or contact electrode poling, a uniform field is very important in order to obtain device quality results. The presence of film nonuniformity caused by impurities or inhomogeneities can reduce the maximum poling field that may be applied before damage occurs. Inhomogeneities may also change the spatial distribution of the effective poling field applied causing local fluctuations in chromophore order and light scattering (poling-induced optical loss).[12]

4.1.1. Conductivity Issues; Buffer Layers

Poling-induced r_{33} is approximately linearly dependent on E_p in the low order limit. Only finite poling field strength may be applied before dielectric breakdown occurs. Therefore, r_{33}/E_p, can be taken as the critical figure-of-merit when comparing EO material performance. The conductivity of a material during poling largely determines the maximum E_p that may be applied at optimum poling temperature. Some newly developed EO materials such as BCOGs display r_{33}/E_p values in the range of 3−5 $(nm/V)^2$, meaning that application of $E_p = 100$ V/μm (a typical value for simple guest−host materials) would yield $r_{33} = 300-500$ pm/V. However, because these materials contain high densities of conjugated EO chromophores, they are typically much more conductive than simple guest−host materials, and maximum E_p is limited. For this reason, reducing conductivity during poling is an important goal.

Poling currents under the application of high poling fields have been shown to be interface limited. Therefore, modification of the electrode/EO material interface with a suitable charge blocking layer can lower the poling current by as much as an order of magnitude.[140] Indeed, recent studies have shown that blocking layers can be applied to the fabrication of hybrid polymer/sol−gel electro-optic modulators yielding improved r_{33} and reduced V_π.[141,142] Further work has shown that deposition of a thin layer ($d \approx 90$ nm) of TiO_2 between the poling electrodes and EO material can reduce poling current and increase r_{33}/E_p by as much as 32%, while allowing the application of a larger maximum E_p.

4.1.2. Laser-Assisted Electric Field Poling

Ordering of azo-dyes using a polarized optical field through a cis−trans photoisomerization mechanism (the Weigert effect) has been demonstrated for photorefractive and nonlinear optical material applications.[143−147] Photoisomerization allows reorientation of the transition dipole moment of the azo-dye until it is oriented perpendicular to the electric field vector of the incident polarized light and optical absorption is minimized. This effect may be combined with electric field poling by introducing an optical field polarized perpendicular to the poling field axis, driving the azo-dye into the poling plane and creating an ordered lattice that is restricted in two dimensions. The symmetry of this two-dimensional order is then broken by the poling field, yielding augmented noncentrosymmetric order. This combination of optical and electric field induced orientation is termed laser-assisted electric field poling (LAPEP).[134] In the case of binary chromophore materials, guest order is coupled to the order of the host, and even cooperative ordering interactions are predicted to exist.[54,134] Therefore, optical field induced enhancement of order in a photoaddressable host material may be transferred to a nonphotoaddressable guest contained within the matrix.

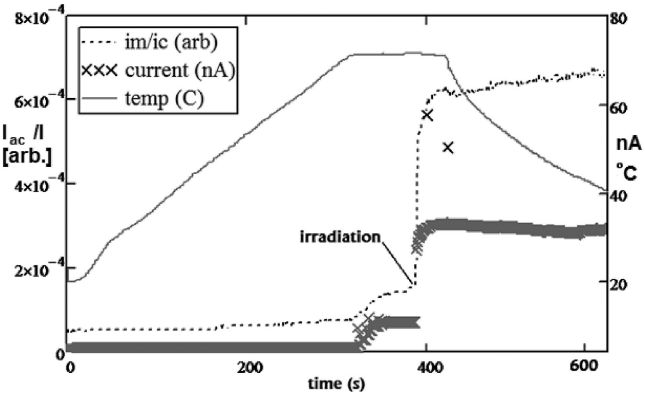

Figure 25. *In situ* plots of the effects of laser-assisted poling on a representative sample of 25% by weight YLD_124 in DR-1-*co*-PMMA are shown (Figure 24b). Parameters plotted include temperature (—), $I_m/I_c \propto r_{33}$ (•••), and current (×××). The point during the poling process at which the pump beam was introduced is denoted as "irradiation". Reprinted with permission from ref 134. Copyright 2008 American Chemical Society.

By LAPEP methods, a 2.5-fold increase in poling efficiency relative to electric field poling has been demonstrated in a binary chromophore system (Figure 24b) consisting of a photoaddressable chromophore host (DR-1-*co*-PMMA) containing a non-photo-addressable guest chromophore (YLD_124). The EO behavior of the system was monitored in real-time using a modified reflection ellipsometry apparatus in order to optimize temperature as well as optical and electrical poling fields.[117,148] Figure 25 shows a representative data trace for LAPEP. Here, "irradiation" denotes the point at which the optical field was introduced and $I_{ac}/I \propto r_{33}$. When the host was ordered using the polarized optical field, electrostatic interactions between the guest and host served to enhance the alignment of the guest chromophore. Due to the limited contribution from the DR-1 chromophore, measurement of r_{33} primarily assessed the order of the guest. Because guest order was insensitive to the application of the optical field, the difference in r_{33}/E_p could be taken as the enhancement effect gained through LAPEP. Under $E_p = 75$ V/μm, using electric field poling only, the EO coefficient was found to be $r_{33} = 50$ pm/V {ATR $\lambda_{exp} = 1.3$ μm}. In contrast, under the same poling field and introducing the polarized optical field ($\lambda_{LAPEP} = 532$ nm; power = 0.1 watts/cm^2) at optimum temperature, $r_{33} = 120$ pm/V {ATR $\lambda_{exp} = 1.3$ μm}. Thus, LAPEP provides a method to augment the acentric order produced by electric field poling and confirms coupling of guest and host order in BCOGs. However, without using interface modification strategies to minimize poling current, the increased photocurrent observed during LAPEP tends to limit the maximum achievable poling field.

4.2. Lattice Hardening and Thermal Stability

Various chemical cross-linking methodologies have been advanced as mechanisms for reducing relaxation subsequent to poling. Several examples of cross-linking chemistry rely on the use of thermally initiated chemical reactions.[13,106,115,123,126,149,150] The resulting thermoset materials cure to form highly cross-linked polymer networks during poling, restricting relaxation. In order for thermosetting chemical reactions to be compatible with the poling process, the cross-linking reactions must take place at a temperature that is just above that of the poling onset temperature, T_p. If cross-linking occurs below poling temperature, poling-induced chromophore orientation will be retarded. Likewise, if the optimum poling temperature is far below that for activation of the cross-linking reaction, poor thermal stability will result. Because of the limited temperature tunability of many of these reactions, initial material (prepoling) T_g must be tuned, for example, by choice of polymer main chain, in order for optimized poling (r_{33}) and cross-linking to occur simultaneously. Despite these considerations, research efforts aimed toward optimizing thermoset schemes have yielded a number of cross-linked materials showing $T_g \geq 200$ °C that maintain large EO coefficients at elevated operating temperatures.[151] The use of the thermally initiated fluorovinyl ether dimerization reaction represents a particularly successful and popular approach (Figure 26a).[80,105,115,150−153]

A novel approach to the problem of cross-linking−poling compatibility was developed by Jen et al. The thermally reversible Diels−Alder reaction was employed to create a thermoplastic material (Figure 26b).[154,155] In this case, a protecting group initially prevented cross-linking before the poling process. At a poling-compatible temperature, the protecting group was removed, and cross-linking occurred as the material cooled, allowing the poling process and the resulting r_{33} to be well optimized. More recently, this Diels−Alder "click" chemistry has been adapted for use in a more traditional thermoset approach with the advantage of a high degree of temperature tunability. Photo-cross-linking methods have also been explored, motivated by the attractive possibility of completely decoupling the poling and curing processes.[127] Effective photo-cross-linking is difficult to achieve due to the high absorption coefficients and relative photosensitivity of many EO chromophores.

5. Characterization Methods

5.1. Methods for Characterizing Molecular First Hyperpolarizability

The two most commonly used methods to characterize molecular first-order hyperpolarizabilities ($\beta_{ijk}(\omega,\varepsilon)$) of EO chromophores in solution are hyper-Rayleigh scattering (HRS)[156−158] and electric field-induced second harmonic generation (EFISH).[159,160] EFISH measures the product of dipole moment and hyperpolarizability, $\mu\beta$, while HRS measures β directly. The HRS technique may also be applied to many different types of EO chromophores such as octupolar, ionic, and dipolar. In contrast, EFISH may only be applied to dipolar chromophores but typically displays better signal-to-noise ratios and can distinguish the sign of β.[12,161]

Several publications report observation of second-harmonic scattering in macroscopically isotropic media along with a theoretical description of the phenomenon.[162−165] Clays and Persoons employed this scattering as a method for determining the first-order hyperpolarizabilities of organic molecules in liquid solution.[160,166] This technique is referred to as HRS. In the HRS experiment, laser light with frequency ω and intensity I_ω is incident on a solution containing the EO chromophore of interest producing scattered light with the frequency, 2ω (second harmonic) of intensity, $I_{2\omega}$. The observed $I_{2\omega}$ is directly related to the orientationally averaged hyperpolarizability, $\beta_{HRS}(-2\omega;\omega,\omega)$, which is a function of ω and the solvent dielectric constant, ε. A typical HRS apparatus for off-resonant HRS measurements is shown in Figure 27.[167,168]

In electric-field-induced second harmonic generation (EFISH) experiments, hyperpolarizability is evaluated by

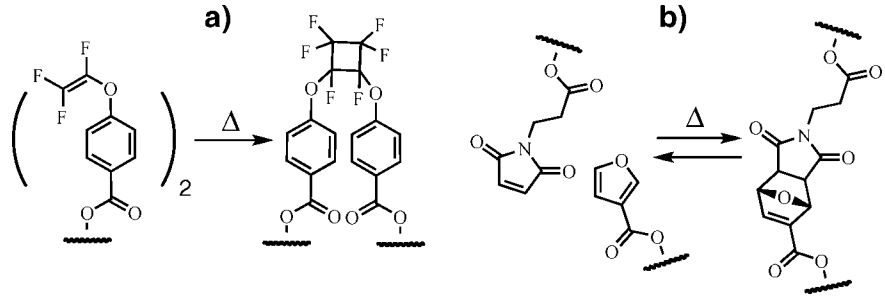

Figure 26. Irreversible fluorovinyl ether dimerization (a) and thermally reversible Diels−Alder (b) cross-linking reactions.

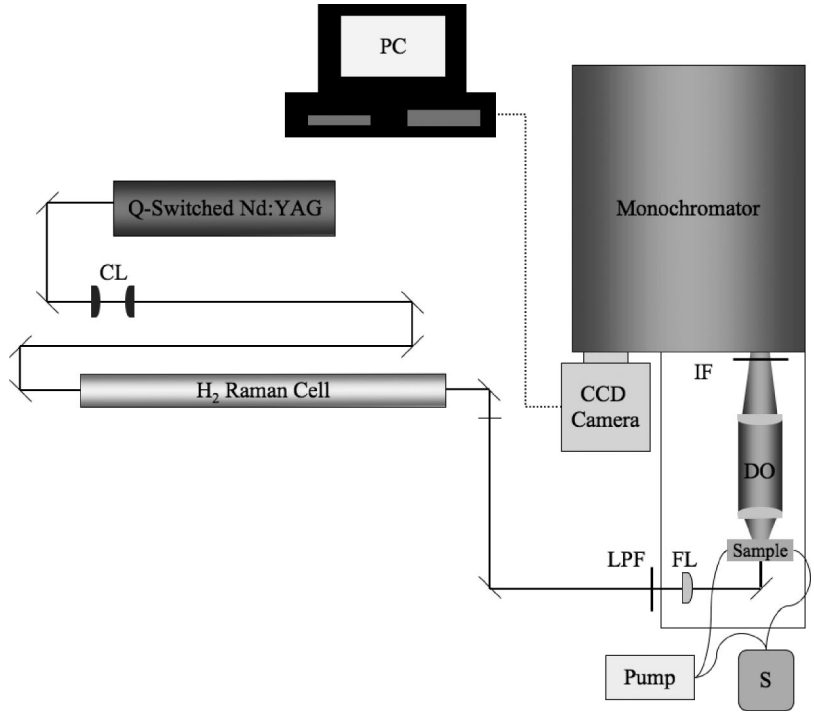

Figure 27. Schematic diagram of a nanosecond-time-response HRS setup (bottom) used for off-resonant HRS measurements.[262] CL = collimating lenses; LPF = long-pass filter; FL = focusing lens; DO = detection (collection) optics.

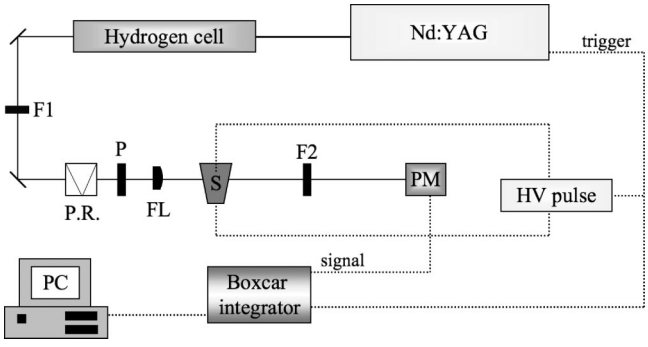

Figure 28. A schematic of the typical EFISH setup. F1 = combination of appropriate filters; P.R. = polarization rotator; P = polarizer aligned parallel to the applied high-voltage field axis; L = focusing lens; S = sample inside the wedged cell on translation stage; F2 = combination of a water cell, interference filter (953 nm), and neutral density filters; HV pulse = high-voltage pulse generator.

measuring $I_{2\omega}$ generated from a chromophore solution under the influence of a strong static electric field. An example of an EFISH setup is shown in Figure 28. Laser light of frequency ω is focused into a wedge-shaped cell, and the coherent second-harmonic intensity, $I_{2\omega}$, is measured. The interaction of the static electric field with the permanent dipoles of the molecules creates a bias in the average orientation of the molecules, resulting in partial acentric dipolar order and inducing intense (relative to HRS), coherent second-harmonic generation.[169] Therefore, $I_{2\omega}$ measured from EFISH is related to the product of the molecular dipole moment, μ, and hyperpolarizability, often given as the molecular figure-of-merit, $\mu\beta$.

HRS and EFISH both exhibit complications that contribute to uncertainty in measured β values.[170−176] For example, absorption by the sample at the fundamental or second harmonic wavelengths (often referred to as *self-absorption*) can attenuate the amount of HRS or EFISH signal produced, thus leading to an underestimation of β. Using Beer−Lambert correction factors, one can minimize this problem as long as the concentration is not too high and, therefore, outside the linear Beer's law regime.[177] More complicated issues include the presence of two-photon absorption, resonance effects, Stokes fluorescence, and two-photon-induced fluorescence (TPF) at the second harmonic wavelength. Several methods have been used to address the problems of Stokes fluorescence and TPF, including spectrally resolving the scattered light, using a picosecond or femtosecond laser to separate the fluorescence in the time domain, or using a high repetition rate femtosecond laser to suppress the fluorescence.[177] Determination of zero-frequency hyperpolarizability, $\beta_{ijk}(0)$, is important in order to perform molecular

comparisons, to compare to theoretical models, and to relate hyperpolarizabilities derived from SHG-based experiments (HRS and EFISH) to values relevant to the EO effect. The simple two-state model (TSM) derived by Oudar and Chemla is widely used to deduce $\beta_{ijk}(0)$ from experimental values.[29] Despite several indications of potential inadequacies associated with these approximations, this model appears to be generally satisfactory for use when measurements are performed far to the low-energy side of resonance.[39,40,177] Newer techniques for assessing frequency dispersion effects include computational modeling techniques such as real-time time-dependent density functional theory (RT-TDDFT).[44]

5.2. Methods for Characterizing Electro-optic Activity

Several different methods exist for characterization of the relevant bulk material electro-optic coefficients including single-beam reflection ellipsometry (Teng−Man technique),[178,179] attenuated total reflection (ATR),[180−182] and two-slit interference.[183] Device operating voltage, V_π (Mach−Zehnder), can also be used to calculate r_{33} of the active material.[12,136] Second harmonic generation (SHG) is yet another method that has been commonly used to evaluate electro-optic coefficients.[184] However, like all SHG measurements (HRS, EFISH), the frequency dispersion relationship of the measured value differs with respect to r_{33}. Therefore, in order to compare this value with those from direct r_{33} measurements, such as Teng−Man, ATR, or device V_π, the two-state approximation must be employed.[29,110] For this reason, SHG measurements are commonly employed for *in situ* monitoring during poling, while a direct measurement is used for determination of r_{33}. The two most common methods for characterization of material r_{33} that are employed for the purpose of routine screening are the Teng−Man technique (TMT) and ATR. Both methods rely on measurement of a change in effective refractive index as a function of applied electric field strength.

The TMT uses a time-varying electric field-induced change in birefringence to create a change in phase angle between surface and plane polarized optical fields of equal intensity. This change in phase angle creates a time-varying change in optical polarization resulting in an output intensity modulation when the light field is passed through a polarizer. This intensity change (measured by lock-in amplifier) is proportional to EO coefficient, and r_{33} may be calculated assuming $r_{33} = 3r_{13}$ (valid for small order parameters). For practical reasons (near-IR absorption by the ITO electrode), it is difficult to perform accurate TMT measurements at wavelengths longer than $\lambda_{exp} = 1.3$ μm. Under certain conditions, TMT measurements may also be complicated by multiple reflections caused by refractive index contrast at interfaces in the multilayer sample.[185] Despite these weaknesses, the TMT is a noncontact technique that requires only basic (relatively inexpensive) optics and low-power diode lasers and is (in principle) simple and fast. The TMT may also be modified to perform real-time relative EO coefficient monitoring while controlling experimental conditions such as temperature and poling field (Figure 29).[118,127,148,186] This technique has been applied to monitor relative EO coefficients *in situ* during laser-assisted poling experiments, allowing simultaneous optimization of multiple experimental parameters. Real-time TMT is also a useful tool with which to assess r_{33} thermal stability.

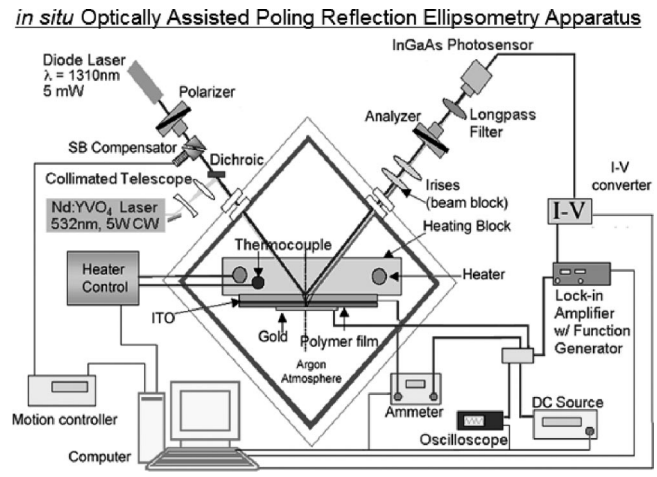

Figure 29. The modified reflection ellipsometry (Teng−Man technique) apparatus for *in situ* monitoring of r_{33} during electric field and laser-assisted poling is shown. Reprinted with permission from ref 134. Copyright 2008 American Chemical Society.

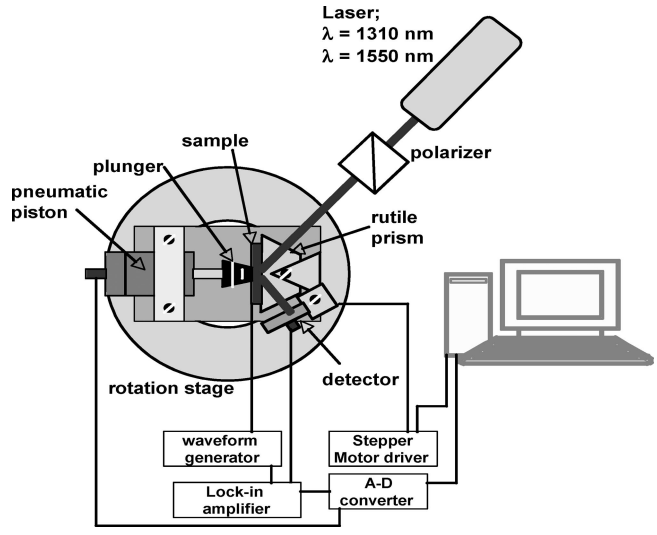

Figure 30. A schematic diagram of the ATR apparatus is shown. Reprinted with permission from ref 37. Copyright 2008 American Chemical Society.

ATR is a prism coupling method that measures a change in the intensity of laser light reflected from the prism/EO film interface as a function of applied electric field. The time-varying refractive index change induced by the application of an ac waveform (the electro-optic effect) causes a time-varying shift in the prism-coupling angle and a change in reflection intensity. The intensity change, measured using a lock-in amplifier, is proportional to the EO coefficient. A schematic of the ATR setup is shown in Figure 30.[37] The sample is mounted on the prism using a pneumatic plunger. The plunger, prism, and detector are mounted atop a stepper motor to allow precise control over the incidence angle of the measurement laser.

Compared with the TMT, the ATR method is relatively slow and is not easily adaptable to *in situ* experiments. ATR is also a contact method in which the poled sample must be mounted onto the prism, risking sample damage. However, because the ATR method only requires the use of a single optical polarization, the electro-optic tensor components, r_{33} and r_{13}, can be measured independently and their ratio correlated to the degree of poling-induced acentric order. ATR also does not suffer from multiple reflection errors or

exhibit a pronounced dependence on electrode properties, allowing straightforward measurements at a variety of laser wavelengths. Additional information such as film thickness and refractive index may also be derived from the data obtained. Recent examples have demonstrated the use of a high index rutile prism (n_0(1310 nm) = 2.462 and n_0(1550 nm) = 2.453), along with incorporation of multiple laser light sources for r_{33} measurements over a range of wavelengths.[37,134] Both of these reports employed a particularly effective strategy for material characterization that used the *in situ* TMT method for optimizing processing conditions followed by subsequent sample analysis using ATR.

5.3. Characterization of Poling-Induced Order: VAPRAS

No experimental techniques currently exist for the direct, independent measurement of $\langle\cos^3\theta\rangle$ in poled EO materials. Therefore, effects on this critical parameter, related to the success of various molecular engineering strategies, have been commonly inferred from changes in r_{33} or SHG, and measurement of the centrosymmetric order parameter $\langle P_2\rangle = (3\langle\cos^2\theta\rangle - 1)/2$. Techniques such as polarized absorption spectroscopy (PAS) permit direct experimental determination of $\langle P_2\rangle$, which can be related to $\langle\cos^3\theta\rangle$ using pseudoatomistic Monte Carlo computer simulations.[63] However, the most commonly used PAS method, in which measurements are only performed at normal incidence (the normal incidence method), has some difficulty distinguishing between poling-induced order and decomposition.[187,188] In order to address this problem, the single polarization variable angle polarized absorption spectroscopy (VAPAS) method was introduced.[189] In this method, the absorption of light polarized parallel to the poling field axis is measured at increasing angles of incidence. These values, adjusted by Snell's law and Fresnel reflection corrections, can then be plotted as a function of $\cos^2\theta$ in order to assess the orientational distribution of the transition dipoles of the EO chromophores within the poled film. The accuracy of the single polarization VAPAS method relies on the modeling of the propagation of light through a complex highly absorbing multiple-interface sample. The original analysis assumed that the complex refractive index components could be treated independently where the real part is treated in terms of Fresnel reflections and Snell's law and the imaginary part in terms of absorbance (order-induced dichroism). Additionally, such modeling does not account for sample inhomogeneities or changes in surface properties caused by the poling (electroding) process.

In order to address the problems associated with simple VAPAS, the variable angle polarization referenced absorption spectroscopy (VAPRAS) method may be employed.[37] In VAPRAS, the ratio of the absorption of light polarized perpendicular to the poling axis (s-polarized) to that of light polarized parallel to the poling axis (p-polarized) is measured as a function of incidence angle. This data may then be analyzed according to

$$\frac{\langle\alpha_f(\lambda_{exp})\rangle_p}{\langle\alpha_f(\lambda_{exp})\rangle_s} = 1 + \sin^2\theta\left(\frac{3r\langle P_2\rangle}{1 - r\langle P_2\rangle}\right) \qquad (14)$$

where $\langle\alpha_f(\lambda_{exp})\rangle_s$ and $\langle\alpha_f(\lambda_{exp})\rangle_p$ are the absorbance of s- and p-polarized light at the experimental wavelength, λ_{exp}, measured at increasing increments of propagation angle. The propagation angle is denoted as θ (with respect to the sample normal), and the anisotropy of the transition dipoles, $r \approx -1$ (in the case of an axial system). The VAPRAS method is essentially able to use $\langle\alpha_f(\lambda_{exp})\rangle_s$ measured at different angles as a reference point because this parameter does not depend on the angle of incidence. It can therefore be used to determine the effective refractive index of the multilayer sample by solving for $d\langle\alpha_f(\lambda_{exp})\rangle_s/d(\cos^2\theta) = 0$, allowing the definition of Snell's law and Fresnel reflection correction factors without prior knowledge of sample thickness or refractive index. This method also largely allows the cancellation of inaccuracies due to surface effects, and sample inhomogeneities. A more rigorous treatment of the VAPRAS data can be performed using the Jones matrix method to model the propagation of electromagnetic radiation through multi-interface materials.[190] By use of polarized absorption spectroscopy methods, poling-induced ordering values have recently been determined for a number of materials at optimum loading densities to be in the range of $\langle P_2\rangle/E_{pol} \approx 0.0004-0.0007$.[37] These measurements may be used in concert with PAMC simulations to estimate $\langle\cos^3\theta\rangle/E_{pol} \approx 0.0016$ for several common prolate-shaped chromophores. This value has been predicted by PAMC modeling to be as high as $\langle\cos^3\theta\rangle/E_{pol} \approx 0.0026$ for dipolar spheroids at low N.[37,63]

5.4. Characterization of Photochemical Stability

Previous investigations into EO material photodegradation processes have suggested that photooxidation and isomerization are primarily responsible for EO material photodecomposition, although other degradation pathways may exist.[191−196] However, the molecular-level mechanism of photo-oxidative damage is still poorly understood.[197] Research aimed toward improving the intrinsic photostability of EO materials must include identification of the fundamental photochemical pathways leading to material photodecomposition. This knowledge may then be used in the design of improved chemical structures.[198]

There are two key methods for determining the photochemical stability of EO materials.[199,200] The first approach is based on a molecular analysis of photodecomposition; a compound undergoes excitation to a higher energy state a certain number of times before decomposition occurs. This allows for the determination of the inverse quantum efficiency for photodegradation, B, which is a wavelength-dependent figure-of-merit that describes photochemical stability of EO materials. Typically, photobleaching measurements that utilize a molecular analysis of photodecomposition are performed on EO chromophores in solution, in thin films, or, as shown recently, in microring resonator devices.[108,201,192,200,66,202] If photodegradation occurs via a single photodecomposition pathway, an estimation of electro-optic chromophore lifetime $\tau = B/(\sigma n)$, can be determined. Here, τ is related to the photon flux at the operational wavelength, and the photostability figure-of-merit, B/σ, which involves the absorption cross-section σ of the chromophore at the same wavelength. Estimations of the B/σ values of EO materials are of major importance for defining material lifetimes. For example, the estimated B/σ of an organic EO compound confined within a channel waveguide having a cross-sectional area of 10 μm^2 operating at 1.55 μm of 1 mW continuous average power would need to be on the order of $B/\sigma \geq 10^{35}$ (or $B \geq 10^9$) in order for this device to reach a lifetime of 10 years.[203]

The second method for measuring and characterizing EO material photostabilities is directly related to device

performance.[103,204,205] Degradation of device performance under operational wavelengths and conditions is monitored, thus providing insight into the stability of the parameters of a functioning device. Devices typically display more complex photodegradation given that oxygen permeation varies depending on the type of device and, more specifically, an oxygen shielding effect may occur due to the buffering of the device layers as well as device packaging. Moreover, photodegradation of other materials (e.g., cladding materials) used in the device may influence the evolution of device performance. However, the device approach to investigating photostability is not practical for material screening (i.e., elucidating structure−property relationships) due to the complexity and expense of the device fabrication process.

Improvements in photostabilities of EO materials have been achieved by various means, including modification of the structures of chromophores and polymer hosts, addition of physical singlet-oxygen quenchers, and device packaging (i.e., oxygen-deficient operating environment).[191,194,195,206,207] As an example, DeRosa et al. studied the effects of EO chromophore photochemical stabilities at 1.55 μm by means of varying molecular structure and demonstrated that chromophore photostability can be enhanced significantly for thienyl-vinylene bridge (FTC)-type and tetraene bridge (CLD)-type systems: the photostability of FTC-type chromophores showed an improvement from a B/σ of 7.1×10^{32} to 23.9×10^{32} m^{-2}, and CLD-type chromophores increased from a B/σ of 1.3×10^{32} to 5.8×10^{32} m^{-2} through chemical structure modification.[206] On the other hand, the photostability figure of merit of a CLD-type chromophore (e.g., CLD-1) was found to vary from $B/\sigma \approx 10^{24}$ to $B/\sigma \approx 10^{26}$ when photobleaching experiments were performed using low- and high-intensity excitation sources at 660 nm (near λ_{max}).[208] When experiments are performed under atmospheric conditions, the photostability figures of merit commonly recorded for most current materials are significantly less than the $B/\sigma \geq 10^{35}$ required for an estimated device lifetime of 10 years. However, $B/\sigma < 10^{35}$ can be achieved under inert (i.e., oxygen-deficient) conditions.[206] Such observations underscore the importance of effective device packaging in order to achieve acceptable device longevity.

Major improvement in EO device stability will most likely result from one or more of the following: addition of an efficient singlet oxygen quencher, protection through the use of a suitable oxygen permeation barrier, chromophore modification to protect reactive sites (α protons), or satisfactory sealed packaging that significantly reduces the potential of photooxidation.

6. Devices and Applications

A wide range of prototype devices relevant to electrical/optical signal transduction,[21,22,87,204,209−221] optical switching (signal routing including wavelength division multiplexing),[21,22,27,28,222−224] phased array radar,[225,226] analog/digital conversion,[227,228] radiofrequency and microwave signal generation,[229] airborne guidance (optical gyroscopes),[230] and digital signal processing[231] have been demonstrated. More complex prototype devices such as high bandwidth acoustic spectrum analyzers have also been demonstrated.[232] Indeed, many more devices and applications relevant to telecommunications, computing, and defense could be cited but lie beyond the scope of this review; however, we would like to call the reader's attention to two application areas that have received little attention in the past but are of growing interest: (1) electro-optic sensors based on ring microresonators[233−247] and (2) terahertz technology applications.[229,248−261] Obviously, organic electro-optic materials are sensors for any phenomenon that results in a change in index of refraction and as such can be used to sense a wide range of physical and chemical phenomena. The most obvious application is the sensing of electromagnetic radiation (from dc to tens of terahertz). Sensing can be either broadband, employing stripline-type sensors, or narrow band employing device structures such as ring microresonators (both all-organic and hybrid organic/silicon photonic structures have been demonstrated).[196−212] Such structures have also been adapted to sense other properties including strain[202] and detection of various chemicals. Stand alone organic ring microresonator devices have been fabricated and have been integrated with side-polished silica fibers to lead to a new generation of fiber sensors. Electro-optic sensors afford the opportunity for the compact integration (including chipscale integration) of sensor, computer processor, and telecommunication (either wireless or fiber optic) capabilities, enabling a variety of embedded network sensing applications. The sensitivity and specificity of such sensors depend on both the selection of sensor material and device design (e.g., the Q factor of nano- to mesoscale ring resonators). Improved sensitivity for the detection of chemical and physical phenomena of interest comes with the cost of increased sensitivity to extraneous factors such as thermal fluctuations. Before current electro-optic sensor technology can be broadly implemented, such performance issues much be addressed; however, devices with a wide range of quality factors (10^3-10^8) can be fabricated, and some athermal designs have already been explored (particularly for all-organic devices). Thus, it is likely that sensors with high sensitivity, controlled bandwidth, and good stability can be achieved.

Exploiting optical rectification, as well as the electro-optic effect, permits generation and detection of terahertz radiation.[213−227] Such capability permits the utilization of terahertz frequencies for spectroscopic and sensing applications. Terahertz radiation is absorbed by the phonon modes of many organic crystals such as plastic explosive materials (RDX, HMX), and thus terahertz spectroscopy is relevant to security screening as well as general spectroscopic applications. Like other forms of electromagnetic radiation (X-rays, IR), the utility of terahertz radiation is determined by its absorption and scattering properties. Potential applications include inspection of semiconductor circuitry and medical imaging. Crystalline inorganic (e.g., ZnTe) and organic materials (e.g., 4-(4-dimethylaminostyryl)-1-methylpyridinium tosylate (DAST) crystals) are alternatives for terahertz generation and detection to electrically poled organic electro-optic materials. However, phonon modes associated with these highly ordered structures limit the bandwidth of the terahertz spectrum that can be utilized, while electrically poled organic electro-optic materials may afford utilization of the full 0.5−30 THz band. The exceptionally large electro-optic coefficients of poled organic electro-optic materials are also an advantage. Finally, poled organic electro-optic materials may facilitate more facile phase matching of optical and terahertz waves permitting longer interaction lengths and, thus, greater sensitivity.

7. Conclusions and Future Prospects

Theory-guided design of organic electro-optic materials has permitted dramatic improvement in properties over the past decade. Electro-optic activity has been increased to

approximately 500 pm/V (in thin, electrically poled films) while keeping optical loss to less than 2 dB/cm and thermal stability (final material glass transition temperature) to greater than 200 °C. Techniques for increasing photochemical stability by more than 4 orders of magnitude have been demonstrated and devices prepared by Lumera Corporation have met Telcordia standards. The recent introduction of binary chromophore organic glass electro-optic materials, laser-assisted electric field poling, and thin metal oxide layers to control charge injection represent promising avenues for further improvement in performance. Indeed, electro-optic activity for organic materials is likely to be increased above 1000 pm/V in the coming years. Such improvement will be important for spatial light modulation and many emerging computing, telecommunications, and sensing applications. The integration of organic nonlinear optical materials (both second- and third-order NLO materials) with silicon photonics is a particularly important achievement of the past 5 years. This may well set the stage for chipscale integration of photonics and electronics, as well as the realization of an important array of new device technologies. The past 5 years has also witnessed the demonstration of important processing and material advantages of organic electro-optic materials including fabrication of complex structures by nanoimprint lithography and demonstration of conformal and flexible devices.

It is unlikely that organic electro-optic materials will replace crystalline electro-optic materials (such as lithium niobate) or electro-absorptive materials (such as gallium arsenide or indium phosphide), nor will organic electro-optic materials eliminate the use of modulated semiconductor lasers. Commercial market penetration by organic electro-optic materials and devices will likely depend on the special properties afforded by these materials including the potential for exceptional bandwidth, drive voltages of less than 0.1 V, ease of manufacture, including the mass production of conformal and flexible devices and the high-density integration of devices, ease of manufacture of three-dimensional optical circuitry, and the ease of integration with nano- to mesoscale silicon photonic circuitry. Organic electro-optic materials and devices also appear to afford superior advantages for airborne and space applications. The compatibility of organic electro-optic materials with very large scale integration (VLSI) semiconductor electronics may be an important advantage for next generation chipscale integration of electronics and photonics relevant to computing, telecommunications, and embedded network sensing. The potential advantages and potential commercial impact of organic electro-optic materials and devices is certainly substantial and could dramatically impact telecommunications, computing, defense, homeland security, transportation, entertainment, medicine, energy (through embedded network sensing), and civil engineering (through new sensors and embedded network sensing). However, the field of organic electro-optics is still immature. Although substantial progress has been made in virtually all areas of research related to this topic (improvement of electro-optic activity, reduction of optical loss, improvement of operational bandwidth, improvement of thermal stability, improvement of photochemical stability, demonstration of new device concepts), these individual advances must still be integrated together into single materials, devices, and systems that capture the attention of end users. Moreover, at this time, problems remain to be addressed regarding cladding and electrode materials. Perhaps new device concepts and circuit options (e.g., silicon photonics) will provide the breakthrough that will enable the large-scale use of organic EO materials. On the positive side, the need for bandwidth (driven by the desire to have video and audio communication capabilities in a single device (e.g., iPhone) and for the delivery either by cable or by wireless of television, music, movies, e-mail, instant messaging, telephone, GPS, etc.,) by a single service provider and the need for reduced drive voltage (driven by RF photonics) will almost certainly drive the implementation of organic electro-optics unless a currently nonexistent competitor materials and device technology is developed. Like silicon photonics, the market for organic electro-optics could be very large indeed, but for both of these new material classes, the extent of commercialization will strongly depend on research progress made in the next 5 years.

An unanticipated benefit of research on organic electro-optic materials has been a better understanding of intermolecular electrostatic interactions, which has led not only to the development of new classes of materials (binary chromophore glasses) but also to new techniques for characterizing nanoscopic order (and thus directly measuring intermolecular electrostatic forces). It is very likely that evolving theoretical methods and experimental techniques will, in the future, provide even greater insight critical to supermolecular (nano- to mesoscopic) engineering. Much as our understanding of molecules grew out of correlated theoretical (quantum mechanics)/experimental studies, our understanding of supermolecular organization is evolving from correlated theoretical (statistical mechanics)/experimental studies. Indeed, electrically poled binary organic glasses and laser-assisted, electrically poled organic glasses provide excellent model systems for the quantitative investigation of guest−host intermolecular electrostatic interactions, which can be systematically tuned by the variation of the structure of the guest and host chromophores.

8. Acknowledgments

The authors gratefully acknowledge financial support provided by the National Science Foundation (Grants DMR-0551020 and DMR-0120967) and by the Air Force Office of Scientific Research (Grant F49620-1-0110-P000). Financial support is also acknowledged from the DARPA MORPH program.

9. References

(1) Burland, D. M., Ed. *Chem. Rev.* **1994**, *94* (1), 1−278.
(2) Prasad, P. N.; Williams, D. J. *Introduction to Nonlinear Optical Effects in Molecules and Polymers*; John Wiley and Sons: New York, 1991.
(3) Hornak, L. A. *Polymers for Lightwave and Integrated Optics*; Marcel Dekker: New York, 1992.
(4) Zyss, J. *Molecular Nonlinear Optics*; Academic: New York, 1994.
(5) Garito, A.; Kajzar, F. *Advances in Nonlinear Optics*; Gordon and Breach: Basel, Switzerland, 1995.
(6) Lindsay, G. A.; Singer, K. D. *Polymers for Second-Order Nonlinear Optics*; American Chemical Society: Washington, DC, 1995.
(7) Nalwa, H. S.; Miyata, S. *Nonlinear Optics of Organic Molecules and Polymers*; CRC Press: Boca Raton, FL, 1997.
(8) Kuzyk, M. G.; Dirk, C. W. *Characterization Techniques and Tabulations for Organic Nonlinear Optical Materials*; Marcel Dekkar: New York, 1998.
(9) Wise, D. L.; Cooper, T. M.; Gresser, J. D.; Trantolo, D. J.; Wnek, G. E. *Electrical and Optical Polymer Systems: Fundamentals, Methods and Applications*; World Scientific: Singapore, 1998.
(10) Dalton, L.; Harper, A.; Ren, A.; Wang, F.; Todorova, G.; Chen, J.; Zhang, C.; Lee, M. *Ind. Eng. Chem. Res.* **1999**, *38*, 8.
(11) Zyss, J. *Chem. Phys.* **1999**, *245*, special issue.

(12) Dalton, L. R. *Adv. Polym. Sci.* **2002**, *158*, 1.
(13) Kajzar, F.; Lee, K. S.; Jen, A. K.-Y. *Adv. Polym. Sci.* **2003**, *161*, 1.
(14) Skotheim, T. A., Reynolds, J. R., Eds. *Handbook of Conducting Polymers. Conjugated Polymers: Theory, Synthesis, Properties, and Characterization*, 3rd ed.; CRC Press: Boca Raton, FL, 2007.
(15) Kim, T.-D.; Luo, J.; Cheng, Y.-J.; Shi, Z.; Hau, S.; Jang, S.-H.; Zhou, X. H.; Tian, Y.; Polishak, B.; Huang, S.; Ma, H.; Dalton, L. R.; Jen, A. K.-Y. *J. Phys. Chem. C* **2008**, *112*, 8091.
(16) Jalali, B.; Fathpour, S. *IEEE J. Lightwave Technol.* **2006**, *24*, 4600.
(17) Xu, Q.; Schmidt, B.; Pradhan, S.; Lipson, M. *Nature* **2005**, *435*, 325.
(18) Schmidt, B.; Xu, Q.; Shakya, J.; Manipatruni, S.; Lipson, M. *Opt. Express* **2007**, *15*, 3140.
(19) Manipatruni, S.; Poitras, C. B.; Xu, Q.; Lipson, M. *Opt. Lett.* **2008**, *33*, 1644.
(20) Liu, A.; Jones, R.; Liao, L.; Samara-Rubio, R. D.; Cohen, O.; Nicolaescu, R.; Paniccia, M. *Nature* **2004**, *427*, 615.
(21) Baehr-Jones, T.; Hochberg, M.; Wang, G.; Lawson, R.; Liao, Y.; Sullivan, P. A.; Dalton, L.; Jen, A. K. Y.; Scherer, A. *Opt. Express* **2005**, *13*, 5216.
(22) Baehr-Jones, T.; Penkov, B.; Huang, J.; Sullivan, P. A.; Davies, J. A.; Takayesu, J.; Luo, J.; Kim, T.-D.; Dalton, L. R.; Jen, A. K.-Y.; Hochberg, M.; Scherer, A. *Appl. Phys. Lett.* **2008**, *92*, 163303.
(23) Song, H.; Oh, M.; Ahn, S.; Steier, W. H. *Appl. Phys. Lett.* **2003**, *82*, 4432.
(24) Huang, Y.; Paloczi, G. T.; Yariv, A.; Zhang, C.; Dalton, L. R. *J. Phys. Chem. B* **2004**, *108*, 8606.
(25) Cox, C. H.; Ackerman, E. I. *J. Phys. Chem. B* **2004**, *108*, 8540.
(26) Dalton, L. R.; Harper, A. W.; Wu, B.; Ghosn, R.; Laquindanum, J.; Liang, Z.; Hubbel, A.; Xu, C. *Adv. Mater.* **1995**, *7*, 519.
(27) Rabiei, P.; Steier, W. H.; Cheng, Z.; Dalton, L. R. *J. Lightwave Technol.* **2002**, *20*, 1968.
(28) Sun, L.; Kim, J. H.; Jang, C. H.; An, D.; Lu, X.; Zhou, Q.; Taboada, J. M.; Chen, R. T.; Maki, J. J.; Tang, S.; Zhang, H.; Steier, W. H.; Zhang, C.; Dalton, L. R. *Opt. Eng.* **2001**, *40*, 1217.
(29) Singer, K. D.; Kuzyk, M. G.; Sohn, J. E. *J. Opt. Soc. Am. B* **1987**, *4*, 968.
(30) Bourhill, G.; Bredas, J. L.; Cheng, L.-T.; Marder, S. R.; Meyers, F.; Perry, J. W.; Tiemann, B. G. *J. Am. Chem. Soc.* **1994**, *116*, 2619.
(31) Brown, E. C.; Marks, T. J.; Ratner, M. A. *J. Phys. Chem. B* **2008**, *112*, 44.
(32) Di Bella, S.; Marks, T. J.; Ratner, M. A. *J. Am. Chem. Soc.* **1994**, *116*, 4440.
(33) Dalton, L. R.; Harper, A. W.; Robinson, B. H. *Proc. Natl. Acad. Sci. U.S.A.* **1997**, *94*, 4842.
(34) Robinson, B. H.; Dalton, L. R. *J. Phys. Chem. A* **2000**, *104*, 4785.
(35) Dalton, L. R.; Robinson, B. H.; Jen, A. K.-Y.; Steier, W. H.; Neilsen, R. *Opt. Mater.* **2003**, *21*, 19.
(36) Sullivan, P. A.; Rommel, H.; Liao, Y.; Olbricht, B. C.; Akelaitis, A. J. P.; Firestone, K. A.; Kang, J. W.; Luo, J.; Davies, J. A.; Choi, D. H.; Eichinger, B. E.; Reid, P. J.; Chen, A.; Jen, A. K. Y.; Robinson, B. H.; Dalton, L. R. *J. Am. Chem. Soc.* **2007**, *129*, 7523.
(37) Davies, J. A.; Elangovan, A.; Sullivan, P. A.; Olbricht, B. C.; Bale, D. H.; Ewy, T. R.; Isborn, C. M.; Eichinger, B. E.; Robinson, B. H.; Reid, P. J.; Li, X.; Dalton, L. R. *J. Am. Chem. Soc.* **2008**, *130*, 10565.
(38) Kanis, D. R.; Ratner, M. A.; Marks, T. J. *Chem. Rev.* **1994**, *94*, 195.
(39) Oudar, J. L.; Chemla, D. S. *J. Chem. Phys.* **1977**, *66*, 2664.
(40) Oudar, J. L. *J. Chem. Phys.* **1977**, *67*, 446.
(41) Marder, S. R.; Perry, J. W.; Bourhill, G.; Gorman, C. B.; Tiemann, B. G.; Mansour, K. *Science* **1993**, *261*, 186.
(42) Marder, S. R.; Gorman, C. B.; Meyers, F.; Perry, J. W.; Bourhil, G.; Bredas, J. L.; Pierce, B. M. *Science* **1994**, *265*, 632.
(43) Kinnibrugh, T.; Bhattacharjee, S.; Sullivan, P.; Isborn, C.; Robinson, B. H.; Eichinger, B. E. *J. Phys. Chem. B* **2006**, *110*, 13512.
(44) Takimoto, Y.; Isborn, C. M.; Eichinger, B. E.; Rehr, J. J.; Robinson, B. H. *J. Phys. Chem. C* **2008**, *112*, 8016.
(45) Chafin, A. P.; Lindsay, G. A. *J. Phys. Chem. C* **2008**, *112*, 7829.
(46) Orr, B. J.; Ward, J. F. *Mol. Phys.* **1971**, *20*, 513.
(47) Kuzyk, M. G. *Phys. Rev. A* **2005**, *72*, 053819.
(48) Meyers, F.; Marder, S. R.; Pierce, B. M.; Bredas, J. L. *J. Am. Chem. Soc.* **1994**, *116*, 10703.
(49) Albert, I. D. L.; Marks, T. J.; Ratner, M. A. *J. Phys. Chem.* **1996**, *100*, 9714.
(50) Albert, I. D. L.; Marks, T. J.; Ratner, M. A. *J. Am. Chem. Soc.* **1997**, *119*, 6575.
(51) Isborn, C.; Leclercq, A.; Vila, F. D.; Dalton, L. R.; Bredas, J. L.; Eichinger, B. E.; Robinson, B. H. *J. Phys. Chem. A* **2007**, *111*, 1319.
(52) Prezhdo, O. V. *Adv. Mater.* **2002**, *14*, 597.
(53) Dalton, L. R.; Sullivan, P. A.; Bale, D. H.; Olbricht, B. C. *Solid-State Electron.* **2007**, *51*, 1263.
(54) Pereverzev, Y. V.; Gunnerson, K. N.; Prezhdo, O. V.; Sullivan, P. A.; Liao, Y.; Olbricht, B. C.; Akelaitis, A. J. P.; Jen, A. K. Y.; Dalton, L. R. *J. Phys. Chem. C* **2008**, *112*, 4355.
(55) Yitzchaik, S.; Marks, T. J. *Acc. Chem. Res.* **1996**, *29*, 197.
(56) van der Boom, M. E.; Marks, T. J. *ACS Symp. Ser.* **2004**, *874*, 30.
(57) Piekara, A. *Proc. R. Soc. London, Ser. A* **1939**, *172*, 360.
(58) Leahy-Hoppa, M. R.; Cunningham, P. D.; French, J. A.; Hayden, L. M. *J. Phys. Chem. A* **2006**, *110*, 5792.
(59) Kim, W.-K.; Hayden, L. M. *J. Chem. Phys.* **1999**, *111*, 5212.
(60) Makowska-Janusik, M.; Reis, H.; Papadopoulos, M. G.; Economou, I. G.; Zacharopoulos, N. *J. Phys. Chem. B* **2004**, *108*, 588.
(61) Chafin, A. P.; Lindsay, G. A. *J. Phys. Chem. C* **2008**, *112*, 7836.
(62) Tu, Y.; Zhang, Q.; Agren, H. *J. Phys. Chem. B* **2007**, *111*, 3591.
(63) Rommel, H. L.; Robinson, B. H. *J. Phys. Chem. C* **2007**, *111*, 18765.
(64) Walsh, C. A.; Burland, D. M.; Lee, V. Y.; Miller, R. D.; Smith, B. A.; Tweig, R. J. *Macromolecules* **1993**, *26*, 3720.
(65) Barto, R. R.; Frank, C. W.; Bedworth, P. V.; Taylor, R. E.; Anderson, W. W.; Ermer, S.; Jen, A. K.-Y.; Luo, J.; Ma, H.; Tang, H.-Z.; Lee, M.; Ren, A. S. *Macromolecules* **2006**, *39*, 7566.
(66) Rezzonico, D.; Jazbinsek, M.; Bosshard, C.; Günter, P.; Bale, D.; Liao, Y.; Dalton, L. R.; Reid, P. J. *J. Opt. Soc. Am. B* **2007**, *24*, 2199.
(67) Staub, K.; Levina, G. A.; Barlow, S.; Kowalczyk, T. C.; Lackritz, H. S.; Barzoukas, M.; Fort, A.; Marder, S. R. *J. Mater. Chem.* **2003**, *13*, 825.
(68) Melikian, G.; Rouessac, F. P.; Alexandre, C. *Synth. Commun.* **1995**, *25*, 3045.
(69) Kang, H.; Evmenenko, G.; Dutta, P.; Clays, K.; Song, K.; Marks, T. J. *J. Am. Chem. Soc.* **2006**, *128*, 6194.
(70) Traber, B.; Wolff, J. J.; Rominger, F.; Oeser, T.; Gleiter, R.; Goebel, M.; Wortmann, R. *Chem.—Eur. J.* **2004**, *10*, 1227.
(71) Wolff, J. J.; Wortmann, R. *Adv. Phys. Org. Chem.* **1999**, *32*, 121.
(72) Zyss, J.; Ledoux, I. *Chem. Rev.* **1994**, *94*, 77.
(73) Wang, Y.; Frattarelli, D. L.; Facchetti, A.; Cariati, E.; Tordin, E.; Ugo, R.; Zuccaccia, C.; Macchioni, A.; Wegener, S. L.; Stern, C. L.; Ratner, M. A.; Marks, T. J. *J. Phys. Chem. C* **2008**, *112*, 8005.
(74) Kang, H.; Facchetti, A.; Jiang, H.; Cariati, E.; Righetto, S.; Ugo, R.; Zuccaccia, C.; Macchioni, A.; Stern, C. L.; Liu, Z.; Ho, S. T.; Brown, E. C.; Ratner, M. A.; Marks, T. J. *J. Am. Chem. Soc.* **2007**, *129*, 3267.
(75) Kang, H.; Facchetti, A.; Jiang, H.; Cariati, E.; Righetto, S.; Ugo, R.; Beverina, L.; Morone, M.; Pagani, G.; Marks, T. J. *Nonlinear Opt., Quantum Opt.* **2006**, *35*, 183.
(76) Kang, H.; Facchetti, A.; Zhu, P.; Jiang, H.; Yang, Y.; Cariati, E.; Righetto, S.; Ugo, R.; Zuccaccia, C.; Macchioni, A.; Stern, C. L.; Liu, Z.; Ho, S. T.; Marks, T. J. *Angew. Chem., Int. Ed.* **2005**, *44*, 7922.
(77) Spraul, B. K.; Suresh, S.; Sassa, T.; Angeles Herranz, M.; Echegoyen; Wada, T.; Perahia, D.; Smith, D. W. *Tetrahedron Lett.* **2004**, *45*, 3253.
(78) Suresh, S.; Zengin, H.; Spraul, B. K.; Sassa, T.; Wada, T.; Smith, J. D. W. *Tetrahedron Lett.* **2005**, *46*, 3913.
(79) Cheng, Y. J.; Luo, J.; Hau, S.; Bale, D. H.; Kim, T. D.; Shi, Z.; Lao, D. B.; Tucker, N. M.; Tian, Y.; Dalton, L. R.; Reid, P. J.; Jen, A. K. Y. *Chem. Mater.* **2007**, *19*, 1154.
(80) Budy, S. M.; Suresh, S.; Spraul, B. K.; Smith, D. W. *J. Phys. Chem. C* **2008**, *112*, 8099.
(81) Jen, A. K. Y.; Cai, Y.; Bedworth, P. V.; Marder, S. R. *Adv. Mater.* **1997**, *9*, 132.
(82) Hu, Z.-Y.; Fort, A.; Barzoukas, M.; Jen, A. K. Y.; Barlow, S.; Marder, S. R. *J. Phys. Chem. B* **2004**, *108*, 8626.
(83) Bedworth, P. V.; Cai, Y.; Jen, A.; Marder, S. R. *J. Org. Chem.* **1996**, *61*, 2242.
(84) Rao, V. P.; Jen, A. K. Y.; Wong, K. Y.; Drost, K. J. *Tetrahedron Lett.* **1993**, *34*, 1747.
(85) Rao, V. P.; Cai, Y. M.; Jen, A. K. Y. *J. Chem. Soc.: Chem. Commun.* **1994**, 1689.
(86) Jen, A. K. Y.; Rao, V. P.; Wong, K. Y.; Drost, K. J. *J. Chem. Soc.: Chem. Commun.* **1993**, 90.
(87) Shi, Y.; Zhang, C.; Zhang, H.; Bechtel, J. H.; Dalton, L. R.; Robinson, B. H.; Steier, W. H. *Science* **2000**, *288*, 119.
(88) Liu, S.; Haller, M. A.; Ma, H.; Dalton, L. R.; Jang, S.-H.; Jen, A. K. Y. *Adv. Mater.* **2003**, *15*, 603.
(89) Luo, J.; Haller, M.; Ma, H.; Liu, S.; Kim, T.-D.; Tian, Y.; Chen, B.; Jang, S.-H.; Dalton, L. R.; Jen, A. K.-Y. *J. Phys. Chem. B* **2004**, *108*, 8523.
(90) He, M. Q.; Leslie, T. M.; Sinicropi, J. A. *Chem. Mater.* **2002**, *14*, 2393.
(91) Liao, Y.; Eichinger, B. E.; Firestone, K. A.; Haller, M.; Luo, J.; Kaminsky, W.; Benedict, J. B.; Reid, P. J.; Jen, A. K. Y.; Dalton, L. R.; Robinson, B. H. *J. Am. Chem. Soc.* **2005**, *127*, 2758.
(92) Liao, Y.; Anderson, C. A.; Sullivan, P. A.; Akelaitis, A. J. P.; Robinson, B. H.; Dalton, L. R. *Chem. Mater.* **2006**, *18*, 1062.
(93) Kim, T.-D.; Kang, J.-W.; Luo, J.; Jang, S.-H.; Ka, J.-W.; Tucker, N.; Benedict, J. B.; Dalton, L. R.; Gray, T.; Overney, R. M.; Park, D. H.; Herman, W. N.; Jen, A. K. Y. *J. Am. Chem. Soc.* **2007**, *129*, 488.

(94) Villemin, D.; Liao, L. *Synth. Commun.* **2001**, *31*, 1771.
(95) Chen, D.; Fetterman, H. R.; Chen, A.; Steier, W. H.; Dalton, L. R.; Wang, W.; Shi, Y. *Appl. Phys. Lett.* **1997**, *70*, 3335.
(96) Mingqian, H.; Leslie, T. M.; Sinicropi, J. A. *Chem. Mater.* **2002**, *14*, 4662.
(97) Rao, V. P.; Jen, A. K. Y.; Chandrasekhar, J.; Namboothiri, I. N. N.; Rathna, A. *J. Am. Chem. Soc.* **1996**, *118*, 12443.
(98) Raposo, M. M. M.; Sousa, A. M. R. C.; Kirsch, G.; Ferreira, F.; Belsley, M.; de Matos Gomes, E.; Fonseca, A. M. C. *Tetrahedron* **2005**, *61*, 11991.
(99) Cai, C.; Bosch, M. M.; Tao, Y.; Muller, B.; Gan, Z.; Kundig, A.; Bosshard, C.; Liakatas, I.; Jager, M.; Gunter, P. *J. Am. Chem. Soc.* **1998**, *120*, 8563.
(100) Raimundo, J.-M.; Blanchard, P.; Frere, P.; Mercier, N.; Ledoux-Rak, I.; Hierle, R.; Roncali, J. *Tetrahedron Lett.* **2001**, *42*, 1507.
(101) Raimundo, J. M.; Blanchard, P.; Gallego-Planas, N.; Mercier, N.; Ledoux-Rak, I.; Hierle, R.; Roncali, J. *J. Org. Chem.* **2002**, *67*, 205.
(102) Hammond, S. R.; Clot, O.; Firestone, K. A.; Bale, D. H.; Lao, D.; Haller, M.; Phelan, G. D.; Carlson, B.; Jen, A. K. Y.; Reid, P. J.; Dalton, L. R. *Chem. Mater.* **2008**, *20*, 3425.
(103) Zhang, C.; Wang, C.; Dalton, L. R.; Zhang, H.; Steier, W. H. *Macromolecules* **2001**, *34*, 253.
(104) Briers, D.; De Cremer, L.; Koekelberghs, G.; Foerier, S.; Verbiest, T.; Samyn, C. *Macromol. Rapid Commun.* **2007**, *28*, 942.
(105) Ma, H.; Liu, S.; Luo, J.; Suresh, S.; Liu, L.; Kang, S. H.; Haller, M.; Sassa, T.; Dalton, L. R.; Jen, A. K.-Y. *Adv. Funct. Mater.* **2002**, *12*, 565.
(106) Zhang, C.; Wang, C.; Yang, J.; Dalton, L. R.; Sun, G.; Zhang, H.; Steier, W. H. *Macromolecules* **2001**, *34*, 235.
(107) Luo, J.; Huang, S.; Cheng, Y.-J.; Kim, T.-D.; Shi, Z.; Zhou, X. H.; Jen, A. K.-Y. *Org. Lett.* **2007**, *9*, 4471.
(108) Cheng, Y.-J.; Luo, J.; Huang, S.; Zhou, X. H.; Shi, Z.; Kim, T.-D.; Bale, D. H.; Takahashi, S.; Yick, A.; Polishak, B. M.; Jang, S.-H.; Dalton, L. R.; Reid, P. J.; Steier, W. H.; Jen, A. K.-Y. *Chem. Mater.* **2008**, *20*, 5047.
(109) Dewar, M. J. S. *J. Chem. Soc.* **1950**, 2329.
(110) Kang, H.; Zhu, P.; Yang, Y.; Facchetti, A.; Marks, T. J. *J. Am. Chem. Soc.* **2004**, *126*, 15974.
(111) Keinan, S.; Zojer, E.; Bredas, J.-L.; Ratner, M. A.; Marks, T. J. *THEOCHEM* **2003**, *633*, 227.
(112) Kang, H.; Facchetti, A.; Stern, C. L.; Rheingold, W. S. K.; Marks, T. J. *Org. Lett.* **2005**, *7*, 3721.
(113) Luo, J.; Ma, H.; Haller, M.; Jen, A. K.-Y.; Barto, R. R. *Chem. Commun.* **2002**, 888.
(114) Gopalan, P.; Katz, H. E.; McGee, D. J.; Erben, C.; Zielinski, T.; Bousquet, D.; Muller, D.; Grazul, J.; Olsson, Y. *J. Am. Chem. Soc.* **2004**, *126*, 1741.
(115) Ma, H.; Chen, B.; Sassa, T.; Dalton, L. R.; Jen, A. K.-Y. *J. Am. Chem. Soc.* **2001**, *123*, 986.
(116) Do, J. Y.; Ju, J. J. *Macromol. Chem. Phys.* **2005**, 1326.
(117) Sullivan, P. A.; Akelaitis, A. J. P.; Lee, S. K.; McGrew, G.; Lee, S. K.; Choi, D. H.; Dalton, L. R. *Chem. Mater.* **2006**, *18*, 344.
(118) Sullivan, P. A.; Olbricht, B. C.; Akelaitis, A. J. P.; Mistry, A. A.; Liao, Y.; Dalton, L. R. *J. Mater. Chem.* **2007**, *17*, 2899.
(119) Kim, T.-D.; Luo, J.; Tian, Y.; Ka, J. W.; Tucker, N. M.; Haller, M.; kang, J. W.; Jen, A. K.-Y. *Macromolecules* **2006**, *39*, 1676.
(120) Kang, H.; Kim, T.-D.; Luo, J.; Haller, M.; Jen, A. K.-Y. *Appl. Phys. Lett.* **2005**, *87*, 071109.
(121) Li, Z.; Zeng, Q.; Li, Z.; Dong, S.; Zhu, Z.; Li, Q.; Ye, C.; Di, C.; Liu, Y.; Qin, J. *Macromolecules* **2006**, *39*, 8544.
(122) Li, Z.; Zeng, Q.; Yu, G.; Li, Z.; Ye, C.; Liu, Y.; Qin, J. *Macromol. Rapid Commun.* **2008**, *29*, 136.
(123) Bai, Y.; Song, N.; Gao, J. P.; Sun, X.; Wang, X.; Yu, G.; Wang, Z. Y. *J. Am. Chem. Soc.* **2005**, *127*, 2060.
(124) Zhu, Z.; Li, Z.; Tan, Y.; Li, Z.; Li, Q.; Zeng, Q.; Ye, C.; Qin, J. *Polymer* **2006**, *47*, 7881.
(125) Li, Z.; Qin, A.; Lam, J. W. Y.; Dong, Y.; Dong, Y.; Ye, C.; Williams, I. D.; Tang, Z. *Macromolecules* **2006**, *39*, 1436.
(126) Luo, J.; Haller, M.; Ma, H.; Liu, S.; Kim, T.-D.; Tian, Y.; Chen, B.; Jang, S.-H.; Dalton, L. R.; Jen, A. K.-Y. *J. Phys. Chem. B* **2004**, *108*, 8523.
(127) Lee, S. K.; Cho, M. J.; Jin, J.-I.; Choi, D. H. *J. Polym. Sci., Part A* **2007**, *45*, 531.
(128) Luo, J.; Haller, M.; Li, H.; Tang, H.-Z.; Jen, A. K.-Y.; Jakka, K.; Chou, C.-H.; Shu, C.-F. *Macromolecules* **2004**, *37*, 248.
(129) Zhu, P.; Kang, H.; Facchetti, A.; Evmenenko, G.; Dutta, P.; Marks, T. J. *J. Am. Chem. Soc.* **2003**, *125*, 11496.
(130) Facchetti, A.; Annoni, E.; Beverina, L.; Morone, M.; Zhu, P.; Marks, T. J.; Pagani, G. A. *Nat. Mater.* **2004**, *3*, 910.
(131) Koch, A. T. H.; Fridrikh, S. V.; Warner, M.; Schwarzwalder, C. E.; Moratti, S. C.; Friend, R. H. *Synth. Met.* **1999**, *101*, 244.
(132) Koeckelberghs, G.; Vangheluwe, M.; Picard, I.; De Groof, L.; Verbiest, T.; Persoons, A.; Samyn, C. *Macromolecules* **2004**, *37*, 8530.
(133) Halter, M.; Liao, Y.; Plocinik, R. M.; Coffey, D. C.; Bhattacharjee, S.; Mazur, U.; Simpson, G. J.; Robinson, B. H.; Keller, S. L. *Chem. Mater.* **2008**, *20*, 1778.
(134) Olbricht, B. C.; Sullivan, P. A.; Wen, G.-A.; Mistry, A.; Davies, J. A.; Ewy, T. R.; Eichinger, B. E.; Robinson, B. H.; Reid, P. J.; Dalton, L. R. *J. Phys. Chem. C* **2008**, *112*, 7983.
(135) Shi, Z.; Luo, J.; Huang, S.; Zhou, X. H.; Kim, T.-D.; Cheng, Y.-J.; Polishak, B. M.; Younkin, T. R.; Block, B. A.; Jen, A. K.-Y. *Chem. Mater.* **2008**, *20*, 6372.
(136) Dalton, L. R.; Harper, A. W.; Ghosn, R.; Steier, W. H.; Ziari, M.; Fetterman, H.; Shi, Y.; Mustacich, R. V.; Jen, A. K. Y.; Shea, K. J. *Chem. Mater.* **1995**, *7*, 1060.
(137) Teng, C. C. In *Nonlinear Optics of Organic Molecules and Polymers*; Nalwa, H. S., Miyata, S., Eds.; CRC Press: Boca Raton, FL, 1997.
(138) Hill, R. A.; Knoesen, A.; Mortazavi, M. A. *Appl. Phys. Lett.* **1994**, *65*, 1733.
(139) Song, R.; Yick, A.; Steier, W. H. *Appl. Phys. Lett.* **2007**, *90*, 191103.
(140) Sprave, M.; Blum, R.; Eich, M. *Appl. Phys. Lett.* **1996**, *69*, 2963.
(141) Enami, Y.; Derose, C. T.; Mathine, D.; Loychik, C.; Greenlee, C.; Norwood, R. A.; Kim, T.-D.; Luo, J.; Tian, Y.; Jen, A. K.-Y.; Peyghambarian, N. *Nat. Photonics* **2007**, *1*, 180.
(142) Enami, Y.; Mathine, D.; Derose, C. T.; Norwood, R. A.; Luo, J.; Jen, A. K.-Y.; Peyghambarian, N. *Appl. Phys. Lett.* **2007**, *91*, 093505.
(143) Donval, A.; Toussaere, E.; Brasselet, S.; Zyss, J. *Opt. Mater.* **1999**, *12*, 215.
(144) Mayer, S. G.; Thomsen, C. L.; Philpott, M. P.; Reid, P. J. *Chem. Phys. Lett.* **1999**, *314*, 246.
(145) Dumont, M.; Hosotte, S.; Froc, G.; Sekkat, Z. *Proc. SPIE* **1994**, *2042*, 2.
(146) Chalupczak, W.; Fiorini, C.; Charra, F.; Nunzi, J.-M.; Raimond, P. *Opt. Commun.* **1996**, *126*, 103.
(147) Zoueu, J. T.; Nunzi, J.-M.; Charra, F. *Opt. Mater.* **2007**, *29*, 468.
(148) Michelotti, F.; Toussaere, E.; Levenson, R.; Liang, J.; Zyss, J. *Appl. Phys. Lett.* **1995**, *67*, 2765.
(149) Song, N.; Men, L.; Gao, J. P.; Bai, Y.; Beaudin, A. M. R.; Yu, G.; Wang, Z. Y. *Chem. Mater.* **2004**, *16*, 3708.
(150) Spraul, B. K.; Suresh, S.; Jin, J.; Smith, D. W. J. *J. Am. Chem. Soc.* **2006**, *128*, 7055.
(151) Dalton, L. R. In *Handbook of Conducting Polymers*, 3rd ed.; Skotheim, T. A., Reynolds, J. R., Eds.; CRC Press: Boca Raton, FL, 2007.
(152) Zhang, C.; Zhang, H.; Oh, M. C.; Dalton, L. R.; Steier, W. H. *Proc. SPIE* **2003**, *4991*, 537.
(153) Ma, H.; Jen, A. K. Y.; Dalton, L. R. *Adv. Mater.* **2002**, *14*, 1339.
(154) Luo, J.; Haller, M.; Li, H.; Kim, T.-D.; Jen, A. K.-Y. *Adv. Mater.* **2003**, *15*, 1635.
(155) Haller, M.; Luo, J.; Li, H.; Kim, T.-D.; Liao, Y.; Robinson, B. H.; Dalton, L. R.; Jen, A. K.-Y. *Macromolecules* **2004**, *37*, 688.
(156) Levine, B. F. *J. Chem. Phys.* **1975**, *63*, 115.
(157) Kajzar, F.; Ledoux, I.; Zyss, J. *Phys. Rev. A* **1987**, *36*, 2210.
(158) Blanchard-Desce, M.; Baudin, J.-B.; Jullien, L.; Lorne, R.; Ruel, O.; Brasselet, S.; Zyss, J. *Opt. Mater.* **1999**, *12*, 333.
(159) Bosshard, C.; Knoepfle, G.; Pretre, P.; Guenter, P. *J. Appl. Phys.* **1992**, *71*, 1594.
(160) Clays, K.; Persoons, A. *Phys. Rev. Lett.* **1991**, *66*, 2980.
(161) Cho, M. J.; Choi, D. H.; Sullivan, P. A.; Akelaitis, A. J. P.; Dalton, L. R. *Prog. Polym. Sci.* **2008**, *33*, 1013.
(162) Giordmaine, J. A. *Phys. Rev.* **1965**, *138*, 1599.
(163) Cyvin, S. J.; Rauch, J. E.; Decius, J. C. *J. Chem. Phys.* **1965**, *43*, 4083.
(164) Bersohn, R.; Pao, Y.-H.; Frisch, H. L. *J. Chem. Phys.* **1966**, *45*, 3184.
(165) Buckingham, A. D.; Orr, B. J. *Q. Rev., Chem. Soc.* **1967**, *21*, 195.
(166) Clays, K.; Persoons, A. *Rev. Sci. Instrum.* **1992**, *63*, 3285.
(167) Firestone, K. A.; Lao, D. B.; Casmier, D. M.; Clot, O.; Dalton, L. R.; Reid, P. J. *Proc. SPIE* **2005**, *5935*, 59350P.
(168) Firestone, K. A.; Reid, P.; Lawson, R.; Jang, S.-H.; Dalton, L. R. *Inorg. Chim. Act.* **2004**, 3957.
(169) Verbiest, T.; Houbrechts, S.; Kauranen, M.; Clays, K.; Persoons, A. *J. Mater. Chem.* **1997**, *7*, 2175.
(170) Stadler, S.; Bourhil, G.; Braeuchle, C. *J. Phys. Chem.* **1996**, *100*, 6927.
(171) Flipse, M. C.; de Jonge, R.; Woudenberg, R. H.; Marsman, A. W.; van Walree, C. A.; Jenneskens, L. W. *Chem. Phys. Lett.* **1995**, *245*, 297.
(172) Song, O. K.; Woodford, J. N.; Wang, C. H. *J. Phys. Chem. A* **1997**, *101*, 3222.
(173) Song, N. W.; Kang, T.-I.; Jeoung, S. C.; Jeon, S.-J.; Cho, B. R.; Kim, D. *Chem. Phys. Lett.* **1996**, *261*, 307.
(174) Song, O.-K.; Wang, C. H. *J. Chem. Phys.* **1996**, *104*, 8230.

(175) Noordman, O. F. J.; van Hulst, N. F. *Chem. Phys. Lett.* **1996**, *253*, 145.
(176) Reis, H. *J. Chem. Phys.* **2006**, *125*, 014506.
(177) Wang, C. H.; Lin, Y. C.; Tai, O. Y.; Jen, A. K. Y. *J. Chem. Phys.* **2003**, *119*, 6237.
(178) Teng, C. C.; Man, H. T. *Appl. Phys. Lett.* **1990**, *56*, 1734.
(179) Schildkraut, J. S. *Appl. Opt.* **1990**, *29*, 2839.
(180) Dentan, V.; Levy, Y.; Dumont, M.; Chastaing, R. E. *Opt. Commun.* **1989**, *69*, 379.
(181) Chen, A.; Chuyanov, V.; Garner, S.; Steier, W. H.; Dalton, L. R. *OSA Tech. Dig. Ser.* **1997**, *14*, 158.
(182) Chen, A.; Chuyanov, V.; Garner, S.; Steier, W. H.; Dalton, L. R. In *Organic Thin Films for Photonic Applications*; Optical Society of America: Washington, DC, 1997; Vol. 14.
(183) Kalluri, S.; Garner, S.; Ziari, M.; Steier, W. H.; Shi, Z.; Dalton, L. R. *Appl. Phys. Lett.* **1996**, *69*, 275.
(184) Becker, M. W.; Sapochak, L. S.; Ghosen, R.; Xu, C.; Dalton, L. R.; Shi, Y.; Steier, W. H.; Jen, A. K.-Y. *Chem. Mater.* **1994**, *6*, 104.
(185) Park, D. H.; Lee, C. H.; Herman, W. N. *Opt. Express* **2006**, *14*, 8866.
(186) Sullivan, P. A.; Akelaitis, A. J. P.; Lee, S. K.; McGrew, G.; Lee, S. K.; Choi, D. H.; Dalton, L. R. *Chem. Mater.* **2006**, *18*, 344.
(187) Rodriguez, V.; Adamietz, F.; Sanguinet, L.; Buffeteau, T.; Sourisseau, C. *J. Phys. Chem. B* **2003**, *107*, 9736.
(188) Mortazavi, M. A.; Knoesen, A.; Kowel, S. T.; Higgins, B. G.; Dienes, A. *J. Opt. Soc. Am. B* **1989**, *6*, 733.
(189) Graf, H. M.; Oliver, Z.; Anthony, J. E.; Dietrich, H. *J. Appl. Phys.* **1994**, *75*, 3335.
(190) Mansuripur, M. *J. Appl. Phys.* **1990**, *67*, 6466.
(191) Galvan-Gonzalez, A.; Canva, M.; Stegeman, G. I.; Twieg, R.; Kowalczyk, T. C.; Lackritz, H. S. *Opt. Lett.* **1999**, *24*, 1741.
(192) Galvan-Gonzalez, A.; Canva, M.; Stegeman, G. I. *Appl. Phys. Lett.* **1999**, *75*, 3306.
(193) DeRosa, M. E.; He, M.; Cites, J. S.; Garner, S. M.; Tang, Y. R. *J. Phys. Chem. A* **2004**, *108*, 8725.
(194) Galvan-Gonzalez, A.; Belfield, K. D.; Stegeman, G. I.; Canva, M.; Marder, S. R.; Staub, K.; Levina, G.; Twieg, R. J. *J. Appl. Phys.* **2003**, *94*, 756.
(195) Galvan-Gonzalez, A.; Canva, M.; Stegeman, G. I.; Sukhomlinova, L.; Twieg, R. J.; Chan, K. P.; Kowalczyk, T. C.; Lackritz, H. S. *J. Opt. Soc. Am. B* **2000**, *17*, 1992.
(196) Galvan-Gonzalez, A.; Belfield, K. D.; Stegeman, G. I.; Canva, M.; Marder, S. R.; Staub, K.; Levina, G.; Twieg, R. J. *J. Appl. Phys.* **2003**, *94*, 756.
(197) Park, S.-J.; Gesquiere, A. J.; Yu, J.; Barbara, P. F. *J. Am. Chem. Soc.* **2004**, *126*, 4116.
(198) Renn, A.; Seelig, J.; Sandoghdar, V. *Mol. Phys.* **2006**, *104*, 409.
(199) Rezzonico, D.; Jazbinsek, M.; Gunter, P.; Bosshard, C.; Bale, D. H.; Liao, Y.; Dalton, L. R.; Reid, P. J. *J. Opt. Soc. Am. B* **2007**, *24*, 2199.
(200) Dubois, A.; Canva, M.; Brun, A.; Chaput, F.; Boilot, J.-P. *Appl. Opt.* **1996**, *35*, 3193.
(201) Zhang, Q.; Canva, M.; Stegeman, G. *Appl. Phys. Lett.* **1998**, *73*, 912.
(202) Bosch, M.; Fischer, C.; Cai, C.; Liakatas, I.; Bosshard, C.; Gunter, P. *Synth. Met.* **2001**, *124*, 241.
(203) Galvan-Gonzalez, A.; Canva, M.; Stegeman, G. I.; Twieg, R.; Chan, K. P.; Kowalczyk, T. C.; Zhang, X. Q.; Lackritz, H. S.; Marder, S.; Thayumanavan, S. *Opt. Lett.* **2000**, *25*, 332.
(204) Zhang, C.; Dalton, L. R.; Oh, M.-C.; Zhang, H.; Steier, W. H. *Chem. Mater.* **2001**, *13*, 3043.
(205) Mortazavi, M. A.; Yoon, H. N.; Teng, C. C. *J. Appl. Phys.* **1993**, *74*, 4871.
(206) DeRosa, M. E.; He, M. Q.; Cites, J. S.; Garner, S. M.; Tang, Y. R. *J. Phys. Chem. B* **2004**, *108*, 8725.
(207) Galvan-Gonzalez, A.; Belfield, K. D.; Stegeman, G. I.; Canva, M.; Chan, K. P.; Park, K.; Sukhomlinova, L.; Twieg, R. J. *Appl. Phys. Lett.* **2000**, *77*, 2083.
(208) Gupta, G.; Steier, W. H.; Liao, Y.; Luo, J.; Dalton, L. R.; Jen, A. K. Y. *J. Phys. Chem. C* **2008**, *112*, 8051.
(209) Kalluri, S.; Chen, A.; Chuyanov, V.; Ziari, M.; Steier, W. H.; Dalton, L. R. *Proc. SPIE* **1995**, 375.
(210) Kalluri, S.; Ziari, M.; Chen, A.; Chuyanov, V.; Steier, W. H.; Chen, D.; Jalali, B.; Fetterman, H. R.; Dalton, L. R. *IEEE Photonics Technol. Lett.* **1996**, *8*, 644.
(211) Shi, Y.; Wang, W.; Bechtel, J. H.; Chen, A.; Garner, S.; Kalluri, S.; Steier, W. H.; Chen, D.; Fetterman, H. R.; Dalton, L. R.; Yu, L. *IEEE J. Sel. Top. Quantum Electron.* **1996**, *2*, 289.
(212) Chen, D.; Fetterman, H. R.; Chen, A.; Steier, W. H.; Dalton, L. R.; Wang, W.; Shi, Y. *Appl. Phys. Lett.* **1997**, *70*, 3335.
(213) Chen, D.; Bhattacharya, D.; Udupa, A.; Tsap, B.; Fetterman, H. R.; Chen, A.; Lee, S. S.; Chen, J.; Steier, W. H.; Dalton, L. R. *IEEE Photonics Technol. Lett.* **1999**, *11*, 54.
(214) Udupa, A. H.; Erlig, H.; Tsap, B.; Cheng, Y.; Chang, D.; Fetterman, H. R.; Zhang, H.; Lee, S. S.; Wang, F.; Steier, W. H.; Dalton, L. R. *Electron. Lett.* **1999**, 35.
(215) Lee, S. S.; Garner, S. M.; Chuyanov, V.; Zhang, H.; Steier, W. H.; Wang, F.; Dalton, L. R.; Udupa, A. H.; Fetterman, H. R. *Quantum Electron.* **2000**, *36*, 527.
(216) Oh, M. C.; Zhang, H.; Szep, A.; Chuyanov, V.; Steier, W. H.; Zhang, C.; Dalton, L. R.; Erlig, H.; Tsap, B.; Fetterman, H. R. *Appl. Phys. Lett.* **2000**, *76*, 3525.
(217) Donval, A.; Toussaere, E.; Hierle, R.; Zyss, J. *J. Appl. Phys.* **2000**, *87*, 3258.
(218) Zhang, H.; Oh, M. C.; Szep, A.; Steier, W. H.; Zhang, C.; Dalton, L. R.; Erlig, H.; Chang, Y.; Chang, D. H.; Fetterman, H. R. *Appl. Phys. Lett.* **2001**, *78*, 3136.
(219) Takayesu, J.; Hochberg, M.; Baehr-Jones, T.; Chang, E.; Wang, G.; Sullivan, P. A.; Liao, Y.; Davies, J. A.; Dalton, L. R.; Scherer, A.; Krug, W. J. *IEEE J. Lightwave Technol.* **2008**, *27*, 440.
(220) Michalak, R. J.; Kuo, Y.-H.; Nash, F. D.; Szep, A.; Caffey, J. R.; Payson, P. M.; Haas, F.; McKeon, B. F.; Cook, P. R.; Brost, G. A.; Luo, J.; Jen, A. K. Y.; Dalton, L. R.; Steier, W. H. *IEEE Photononics Technol. Lett.* **2006**, *18*, 1207.
(221) Oh, M. C.; Zhang, H.; Zhang, C.; Erlig, H.; Chang, Y.; Tsap, B.; Chang, D.; Szep, A.; Steier, W. H.; Fetterman, H. R.; Dalton, L. R. *IEEE J. Sel. Top. Quantum Electron.* **2001**, *7*, 826.
(222) An, D.; Shi, Z.; Sun, L.; Taboada, J. M.; Zhou, Q.; Lu, X.; Chen, R. T.; Tang, S.; Zhang, H.; Steier, W. H.; Ren, A. S.; Dalton, L. R. *Appl. Phys. Lett.* **2000**, *76*, 1972.
(223) An, D.; Tang, S.; Shi, Z.; Sun, L.; Taboada, J. M.; Zhou, Q.; Lu, X.; Chen, R. T.; Zhang, H.; Steier, W. H.; Ren, A. S.; Dalton, L. R. *Proc. SPIE* **2000**, *3950*, 90.
(224) Bechtel, J. H.; Shi, Y.; Zhang, H.; Steier, W. H.; Zhang, C. H.; Dalton, L. R. *Proc. SPIE* **2000**, *4114*, 58.
(225) Lee, S. S.; Udupa, A. H.; Erlig, H.; Zhang, H.; Chang, Y.; Zhang, C.; Chang, D. H.; Bhattacharya, D.; Tsap, B.; Steier, W. H.; Dalton, L. R.; Fetterman, H. R. *IEEE Microwave Guided Wave Lett.* **1999**, *9*, 357.
(226) Fetterman, H. R.; Chang, D.; Steier, W. H.; Dalton, L. R.; Zhang, C.; Oh, M.; Erlig, H.; Tsap, B. *Opt. Soc. Am. Tech. Dig.* **2000**, 146.
(227) Chang, D. H.; Erlig, H.; Oh, M. C.; Zhang, C.; Steier, W. H.; Dalton, L. R.; Fetterman, H. R. *IEEE Photonics Technol. Lett.* **2000**, *12*, 537.
(228) Fetterman, H. R.; Chang, D. H.; Erlig, H.; Oh, M.; Zhang, C. H.; Steier, W. H.; Dalton, L. R. *Proc. SPIE* **2000**, *4114*, 44.
(229) Fetterman, H. R.; Udupa, A.; Bhattachaya, D.; Erlig, H.; Ali, M.; Chang, Y.; Dalton, L. R. *Terahertz Electron. Proc.* **1998**, 102.
(230) Lindsay, G. A., private communication.
(231) Fetterman, H. R. In *High Speed Photonic Devices*; Dagli, N., Ed.; Taylor and Francis: New York, 2006.
(232) Yacoubian, A.; Chuyanov, V.; Garner, S. M.; Steier, W. H.; Ren, A. S.; Dalton, L. R. *IEEE Sel. Top. Quantum Electron.* **2000**, *6*, 810.
(233) Sherwood, T.; Young, A. C.; Takayesu, J.; Jen, A. K.-Y.; Dalton, L. R.; Chen, A. *IEEE Photonics Technol. Lett.* **2005**, *17*, 2107.
(234) Chen, A.; Sun, H.; Pyayt, A.; Young, A. C.; Jen, A. K.-Y.; Takayesu, J.; Dalton, L. R. *IEEE Sensors* **2005**, 735.
(235) Sun, H.; Pyayt, A.; Luo, J.; Shi, Z.; Hau, S.; Jen, A. K.-Y.; Dalton, L. R.; Chen, A. *Proc. SPIE* **2006**, *6117*, 611713.
(236) Zhou, J.; Pyayt, A.; Dalton, L. R.; Luo, J.; Jen, A. K.-Y.; Chen, A. *IEEE Photonics Technol. Lett.* **2006**, *18*, 2221.
(237) Chen, A.; Dalton, L. R.; Sherwood, T. J.; Jen, A. K.-Y.; Robiei, P.; Steier, W. H.; Huang, Y.; Paloczi, G. T.; Poon, J. K.; Scherer, A.; Yariv, A. *Proc. SPIE* **2005**, *5708*, 187.
(238) Shi, Z.; Hau, S.; Luo, J.; Kim, T. D.; Tucker, N. M.; Ka, J. W.; Sun, H.; Pyayt, A.; Dalton, L. R.; Chen, A.; Jen, A. K. Y. *Adv. Funct. Mater.* **2007**, *17*, 2557.
(239) Bhola, B.; Song, H. C.; Tarawa, H.; Steier, W. H. *IEEE Photonics Technol. Lett.* **2005**, *17*, 867.
(240) Sun, H.; Pyayt, A.; Luo, J.; Shi, Z.; Hau, S.; Jen, A. K. Y.; Dalton, L. R.; Chen, A. *Proc. SPIE* **2006**, *6117*, 611713.
(241) Sun, H.; Pyayt, A.; Luo, J.; Shi, Z.; Hau, S.; Jen, A. K. Y.; Dalton, L. R.; Chen, A. *IEEE Sensors J.* **2007**, *7*, 515.
(242) Pyayt, A.; Zhang, X.; Luo, J.; Jen, A. K. Y.; Dalton, L. R.; Chen, A. *Proc. SPIE* **2007**, *6556*, 65561D.
(243) Sun, H.; Chen, A.; Olbricht, B. C.; Davies, J. A.; Sullivan, P. A.; Liao, Y.; Dalton, L. R. *Appl. Phys. Lett.* **2008**, *92*, 193305.
(244) Sun, H.; Chen, A.; Olbricht, B. C.; Davies, J. A.; Sullivan, P. A.; Liao, Y.; Dalton, L. R. *Opt. Express* **2008**, *16*, 6592.
(245) Sun, H.; Chen, A.; Olbricht, B. C.; Davies, J. A.; Sullivan, P. A.; Liao, Y.; Shi, Z.; Luo, J.; Jen, A. K. Y.; Dalton, L. R. *Opt. Express* **2008**, *16*, 8472.
(246) Chen, A.; Sun, H.; Pyayt, A.; Dalton, L. R.; Luo, J.; Jen, A. K. Y. *IEEE J. Sel. Top. Quantum Electron.* **2008**, *14*, 1281.
(247) Pyayt, A.; Wiley, B.; Xia, Y.; Chen, A.; Dalton, L. R. *Nat. Nanotechnol.* **2008**, *3*, 660.

(248) Sinyukov, A. M.; Hayden, L. M. *J. Phys. Chem. B* **2004**, *108*, 8515.
(249) Sinyukov, A. M.; Leahy, M. R.; Hayden, L. M.; Haller, M.; Luo, J.; Jen, A. K. Y.; Dalton, L. R. *Appl. Phys. Lett.* **2004**, *85*, 5827.
(250) Schneider, A.; Gunter, P. **2005**, *318*, 83.
(251) Kawase, K.; Hatanaka, T.; Takahashi, H.; Nakamura, K.; Taniuchi, T.; Ito, H. *Opt. Lett.* **2000**, *25*, 1714.
(252) McLaughin, C. V.; Hayden, L. M.; Polishak, B.; Huang, S.; Luo, J.; Kim, T.-D.; Jen, A. K. Y. *Appl. Phys. Lett.* **2008**, *92*, 151107.
(253) Cunningham, P. D.; Hayden, L. M. *J. Phys. Chem. C* **2008**, *112*, 7928.
(254) McLaughin, C. V.; Zheng, X.; Hayden, L. M. *Appl. Opt.* **2007**, *46*, 6283.
(255) Zurk, L. M.; Orlowski, B.; Jouni, B.; Winebrenner, D. P.; Thorsos, E. I.; Leahy-Hoppa, M. R.; Hayden, L. M. *J. Opt. Soc. Am. B* **2007**, *24*, 2238.
(256) Zheng, X.; McLaughin, C. V.; Cunningham, P.; Hayden, L. M. *J. Nanoelectron. Optoelectron.* **2007**, *2*, 58.
(257) Leahy-Hoppa, M. R.; Fitch, M. J.; Zheng, X.; Hayden, L. M. *Chem. Phys. Lett.* **2007**, *434*, 227.
(258) Zheng, X.; Sinyukov, A.; Hayden, L. M. *Appl. Phys. Lett.* **2005**, *87*, 081115.
(259) Sinyukov, A. M.; Hayden, L. M. *J. Phys. Chem. B* **2004**, *108*, 5815.
(260) Hayden, L. M.; Sinyukov, A. M.; Leahy, M. R.; Lindahl, P.; French, J.; Herman, W.; He, M.; Tweig, R. J. *J. Polym. Sci., Part B: Polym. Phys.* **2003**, *41*, 2492.
(261) Sinyukov, A. M.; Hayden, L. M. *Opt. Lett.* **2002**, *27*, 55.
(262) Firestone, K. A. University of Washington, 2005.

CR9000429